HHS Public Access

Author manuscript

Dev Cell. Author manuscript; available in PMC 2019 June 05.

Published in final edited form as:

Dev Cell. 2018 September 10; 46(5): 627–640.e5. doi:10.1016/j.devcel.2018.07.020.

Glycan-independent Gamete Recognition Triggers Egg Zinc Sparks and ZP2 Cleavage to Prevent Polyspermy

Keizo Tokuhiro[1,2] and **Jurrien Dean**[1,3,*]

[1]Laboratory of Cellular and Developmental Biology, NIDDK, National Institutes of Health, Bethesda, MD 20892, USA

[2]Present address: Department of Genome Editing, Institute of Biomedical Science, Kansai Medical University, 2-5-1 Shinmachi, Hirakata, Osaka 573-1010, Japan

[3]Lead contact

SUMMARY

The zona pellucida surrounding ovulated eggs regulates monospermic fertilization necessary for successful development. Using mouse transgenesis, we document that the N-terminus of ZP2 is sufficient for sperm binding to the zona matrix and for *in vivo* fertility. Sperm binding is independent of ZP2 glycans and does not occur after complete cleavage of ZP2 by ovastacin, a zinc metalloendopeptidase stored in egg cortical granules. Immediately following fertilization, a rapid block to sperm penetration of the zona pellucida is established that precedes ZP2 cleavage but requires ovastacin enzymatic activity. This block to penetration is associated with release of zinc from cortical granules coincident with exocytosis. High levels of zinc affect forward motility of sperm to prevent their passage through the zona matrix. This transient, post-fertilization block to sperm penetration provides a temporal window to complete the cleavage of ZP2 which prevents sperm binding to ensure monospermy.

INTRODUCTION

The successful onset of development depends on the ability of sperm to bind and penetrate the extracellular zona pellucida surrounding eggs, but not embryos, which ensures monospermic fertilization (Wong and Wessel, 2006; Avella et al., 2013; Okabe, 2013). Mouse and human zonae pellucidae contain three and four glycoproteins (ZP1–4), respectively (Bleil and Wassarman, 1980b; Bauskin et al., 1999) and zona glycans have been implicated in gamete recognition (for review, see Yonezawa, 2014). A single genetic locus encodes each zona protein in mouse and human genomes. Genetic ablation of *Zp1* decreases fecundity, but female mice form a zona matrix and are fertile (Rankin et al., 1999). Mouse *Zp4* is a pseudogene (Lefièvre et al., 2004) and human ZP4 is not sufficient to support human sperm binding in transgenic mice (Yauger et al., 2011). Thus, neither ZP1 nor ZP4

*Correspondence: jurrien.dean@nih.gov.

AUTHOR CONTRIBUTIONS

K.T. and J.D. designed the experiments, analyzed the data, and wrote the paper. K.T. performed the experiments.

DECLARATION OF INTERESTS

The authors declare no competing interests.

appear essential for sperm-egg interactions and fertility. ZP2 and ZP3 are common to all vertebrate zonae and each has been proposed as a zona ligand for sperm binding (Bleil and Wassarman, 1980a; Tian et al., 1997). However, no zona matrix is present surrounding ovulated eggs after genetic ablation of *Zp2* or *Zp3* which initially precluded meaningful *in vivo* evaluation of either as a sperm binding ligand (Liu et al., 1996; Rankin et al., 1996; Rankin et al., 2001).

More recent gain-of-function and loss-of-function assays in genetically engineered mice, have implicated ZP2 as the primary ligand for human and mouse sperm binding to the zona pellucida (Baibakov et al., 2012; Avella et al., 2014). Following fertilization, mature $ZP2^{35-633}$ is cleaved near its N-terminus by ovastacin, an egg cortical granule astacin-like metalloendopeptidase encoded by *Astl*. Sperm do not bind to the zona matrix surrounding two-cell embryos. Mutation of the ZP2 cleavage site ($^{167}LA^{\downarrow}DE^{170}$) or genetic ablation of *Astl* maintains ZP2 intact and mouse sperm bind to the zona pellucida even after fertilization and cortical granule exocytosis (Gahlay et al., 2010; Burkart et al., 2012). In loss-of-function assays, mice lacking $ZP2^{51-149}$ form a zona matrix, but are infertile after natural mating (Avella et al., 2014). The interpretation of these observations has been controversial and whether the loss of fertility in the absence of the N-terminus of ZP2 was a direct or indirect effect on gamete recognition was not determined. Nor did these investigations experimentally address an essential role for glycans in sperm-zona interactions which long has been a central tenet of the molecular basis of gamete interactions (Abou-Haila et al., 2014; Chiu et al., 2014; Clark, 2014).

Using mouse transgenesis, we now report that $moZP2^{35-149}$ or $moZP2^{35-262}$ fused to the N-terminus of huZP4 is sufficient for sperm binding and fertility in the absence of native ZP2. Oglycans are not detected in native mouse ZP2 (Boja et al., 2003) and $Zp2^{N83Q}$ mutant mice lacking the single N-glycan in this region are fertile. Thus, neither N- nor O-glycans are required for sperm binding to the N-terminus of ZP2 and for *in vivo* fertility. We further document that following fertilization, there is a rapid block to sperm penetration of the zona matrix that is transient, dependent on the enzymatic activity of ovastacin and is associated with release of cortical granule zinc that affects sperm motility. Subsequently, ovastacin cleavage of ZP2 provides a permanent block to sperm binding and ensures monospermic fertilization.

RESULTS

Sperm bind to $moZP2^{35-149}$/huZP4 and $moZP2^{35-262}$/huZP4 fusion proteins in the absence of native ZP2

Mouse ZP2 contains 713 amino acids, including a signal peptide (1–34 aa), a zona module (364–630 aa), a transmembrane domain (684–703 aa) and a short cytoplasmic tail (704–713 aa). After processing and secretion, mature ZP2 (35–633 aa) associates with ZP1 and ZP3 in forming the extracellular zona pellucida. DNA recombineering was used to clone transgenes that contained genomic DNA encoding either mouse $ZP2^{35-149}$ (mo*Zp2* exons 2–5) or mouse $ZP2^{35-262}$ (mo*Zp2* exons 2–9) inserted into hu*ZP4* exon 1 (Figures 1A, S1A and S1B). Pronuclear injection of the transgenes was used to establish >2 mouse lines for each construct. Expression of each transgene was controlled by 2.5 kb of the 5' hu*ZP4* promoter

and founders for each of the two lines were designated mo*Zp2*$^{35-149}$/hu*ZP4* or mo*Zp2*$^{35-262}$/hu*ZP4*. Mo*Zp2*/hu*ZP4* fusion transcripts were detected by RT-PCR in ovaries, but not 8 other tissues (Figure S1C). The fusion proteins, lacking the moZP2$^{1-34}$ signal peptide, were directed into the secretory pathway by the huZP4$^{1-18}$ signal peptide.

Zp2^{Null} mouse lines have been characterized previously and form a vanishingly thin zona pellucida surrounding ovarian oocytes. A zona matrix is not detected in ovulated eggs and homozygous *Zp2*^{Null} female mice are infertile (Rankin et al., 2001). Expression of either mo*Zp2*$^{35-149}$/hu*ZP4* or mo*Zp2*$^{35-262}$/hu*ZP4* rescues the abnormal *Zp2*^{Null} morphology. A zona pellucida was present surrounding intraovarian oocytes and ovulated eggs. However, in each case, the reconstituted zona pellucida was thinner than normal. Therefore, these lines were crossed with hu*ZP4* transgenic mice to provide a more robust zona matrix (Figures 1B and 1C; see Table S1 for genotypes of mice used in these studies). Using domain specific monoclonal antibodies, the N-terminus, but not the C-terminus of moZP2 was detected in the zona pellucida surrounding ovulated eggs from the two transgenic lines as were moZP1, moZP3 and huZP4 proteins (Figure 1C).

Capacitated mouse sperm bound well to the zona pellucida of mo*Zp2*$^{35-149}$/hu*ZP4* and mo*Zp2*$^{35-262}$/hu*ZP4* rescue eggs (Table S1) using *Zp3*^{EGFP} eggs (Zhao et al., 2002) and two-cell embryos as positive and negative wash controls, respectively (Figure 1D). The cumulus, derived from ovarian follicles, is a mass of hyaluronan interspersed with granulosa cells that surrounds ovulated eggs in the oviduct (Yanagimachi, 1994). Rescue eggs in cumulus (Figure 1E) or after treatment with hyaluronidase to remove the cumulus (Figure 1F) were isolated and inseminated with sperm (5×10^5 ml^{-1}). Wildtype eggs were positive controls and hu*ZP4* transgenic mice in a mo*Zp2*^{Null} background that form a zona matrix to which sperm will not bind (Yauger et al., 2011) were used as negative controls. In each case, mo*Zp2*$^{35-149}$/hu*ZP4* and mo*Zp2*$^{35-262}$/hu*ZP4* rescue eggs were fertilized at rates comparably to wildtype eggs. These studies were extended by *in vivo* matings where 41.3 ± 4.2% and 53.5 ± 2.0%, respectively, of eggs from mo*Zp2*$^{35-149}$/hu*ZP4* and mo*Zp2*$^{35-262}$/hu*ZP4* female mice were fertilized when flushed from oviducts 22 hr after the administration of hCG. Half (3 out of 6) of the mo*Zp2*$^{35-149}$/hu*ZP4* and 60% (3 out of 5) of the mo*Zp2*$^{35-262}$/hu*ZP4* female mice produced litters which were smaller than controls (Figure 1G and Table S1). From these results, we conclude that the N-terminus of mouse ZP2 is sufficient for sperm binding *in vitro* and fertility occurs *in vivo*, albeit with decreased fecundity.

Mo*Zp2*^{N83Q} mice lacking glycans in the N-terminus of ZP2 support sperm binding and are fertile

There has been considerable investigative interest in the role of glycans in mediating the binding of sperm to the zona pellucida. Earlier microscale mass spectrometry studies did not detect O-glycans on native mouse ZP2, but did detect six N-glycans (Boja et al., 2003), one of which (ZP2^{N83}) is in the N-terminal sperm binding domain (Avella et al., 2014). Therefore, two additional transgenic mouse lines were established using site-directed mutagenesis of pre-existing transgenes (Figures S1D–S1F). In each, the genomic DNA sequence was mutated to prevent N-glycosylation of the N-terminal site. Mo*Zp2*^{N83Q}

encoded otherwise intact moZP2 and mo*Zp2*$^{35-149(N83Q)}$/hu*ZP4* encoded the described moZP2$^{35-149}$/huZP4 fusion protein (Figures 2A and S2A).

After mo*Zp2*^{N83Q} was crossed into the *Zp2*^{Null} background, a robust zona pellucida was formed surrounding intraovarian oocytes (Figure 2B). Monoclonal antibodies specific to the N- or C-termini of moZP2 were used to compare zonae pellucidae from wildtype and mo*Zp2*^{N83Q} ovulated eggs and two-cell embryos on immunoblots (Figure 2C, left panel; see Figure S4 for uncropped images). The C-terminus mAb (m2c.2) detected a decrease in gel mobility of intact ZP2^{N83Q} in eggs consistent with the anticipated loss of a single N-glycan. After fertilization, ZP2 is cleaved at ^{167}LA$^{\downarrow}$DE^{170}. No change in gel mobility was observed in the zonae from two-cell embryos which indicated that the lost N-glycan was present on N-terminus ZP2$^{35-168}$. This was confirmed with an mAb to the N-terminus of ZP2 (IE-3) which detected a heterogeneous band (~20–30kD) in wildtype and a single band (~15kD) in zonae from homozygous mo*Zp2*^{N83Q} mutant two-cell embryos (Figure 2C, right panel). Using immunoblots and the mAb to the N-terminus before and after treatment with N-glycanase (Figure 2D), confirmed that the heterogeneity observed in the N-terminus fragment was due to the presence of N-glycan isoforms. Capacitated mouse sperm bound robustly to ovulated eggs in an *in vitro* sperm binding assay using *Zp3*^{EGFP} eggs and two-cell embryos as positive and negative wash controls, respectively (Figure 2E). Homozygous mo*Zp2*^{N83Q} mutant mice in a *Zp2*^{Null} background had near-normal *in vitro* and *in vivo* fertility (Figure 2F, Table S1).

Similar investigations were undertaken with homozygous mo*Zp2*$^{35-149(N83Q)}$/hu*ZP4* mice (Figure S2A) in a mo*Zp2*^{Null} background. Like mo*Zp2*$^{35-149}$/hu*ZP4* and mo*Zp2*$^{35-262}$/hu*ZP4* females, the zona pellucida was thinner than normal. However, after crossing with huZP4 transgenic mice, a zona matrix surrounding intraovarian oocytes and ovulated eggs was reconstituted in the absence of endogenous mouse ZP2 (Figures S2B and S2C). Using domain specific mAb, the N-terminus, but not the C-terminus of moZP2 was detected in the zona pellucida of ovulated eggs from homozygous mo*Zp2*$^{35-149(N83Q)}$/hu*ZP4* mice along with moZP1, moZP3 and huZP4 proteins (Figure S2C). Sperm bound well to the zona matrix containing the moZP2$^{35-149(N83Q)}$/huZP4 fusion protein using hu*ZP4* rescue eggs (Avella et al., 2014) as a negative control (Figure S2D). Homozygous mo*Zp2*$^{35-149(N83Q)}$/hu*ZP4* rescue eggs were fertilized *in vitro* in the absence of cumulus (Figure S2E) as well as *in vivo* (Figure S2F), although not as robustly as wildtype. Taken together, we conclude that the previously observed heterogeneity of the N-terminus fragment containing the sperm binding domain (Burkart et al., 2012) is due to N-glycosylation and that neither N- nor O-glycans in this region are essential for sperm binding and fertility.

Establishment of a transient, post-fertilization block to sperm penetration of the zona matrix

Following fertilization, peripherally located cortical granules fuse with the egg plasma membrane and release ovastacin, a zinc metalloendopeptidase (Quesada et al., 2004), which cleaves ZP2 (Burkart et al., 2012). Normally, mouse sperm do not bind to the zona pellucida surrounding two-cell embryos (Inoue and Wolf, 1975). However, after mutation of the ZP2 cleavage site (^{167}LA$^{\downarrow}$DE^{170} → ^{167}LGAA^{170}), mouse sperm will bind to the zona pellucida

surrounding two-cell embryos, despite fertilization and cortical granule exocytosis (Gahlay et al., 2010).

The post-fertilization cleavage of ZP2 is not immediate. Following *in vitro* insemination, complete cleavage of ZP2 takes ~4 hr at which time ~90% of the eggs have been fertilized and subsequently develop 2 pronuclei (Figure 3A). Despite the presence of thousands of sperm under these experimental conditions, polyspermy (>1 sperm within the egg cytoplasm) or even supernumerary sperm in the perivitelline space (PVS) is not common. Activation of eggs with strontium chloride provides a more precise temporal window of post-fertilization effects on the zona pellucida. Under these experimental conditions, complete cleavage of ZP2 occurs within 30 min of egg activation (Figure 3B). Nevertheless, neither supernumerary sperm in the PVS nor polyspermy were common which suggests a block to sperm penetration prior to complete ZP2 cleavage.

To determine the relationship of the block to sperm penetration with the permanent block to sperm binding imposed by cleavage of ZP2, we used the $Zp2^{Mut}$ rescue mice (Gahlay et al., 2010) crossed with hu*ZP4* transgenic mice to provide a more robust zona pellucida. $Zp2^{Mut}$ rescue eggs were activated with strontium chloride and sperm insemination was delayed for up to 5 hr after which eggs were incubated for an additional 6 hr, fixed and imaged (Figure 3C). Few sperm were present in the perivitelline space if insemination was delayed for 0–2 hr, but increasing numbers of sperm accumulated in the PVS if insemination was delayed ≥ 3 hr (Figure 3D). This suggested that there is a transient block to sperm penetration of the zona pellucida that is triggered by fertilization and begins to dissipate by 9 hr after egg activation.

To investigate further, ovulated eggs, two- and four-cell embryos were isolated from wildtype and $Zp2^{Mut}$ female mice, inseminated with capacitated sperm for 6 hr, fixed and imaged (Figure 3E). Sperm were not observed in the PVS of wildtype eggs, two- or four-cell embryos. Relatively few sperm were present in the PVS of $ZP2^{Mut}$ eggs, but ≥ 15 sperm were present in the PVS of two- or four-cell embryos (Figure 3F). From these observations we conclude that the transient block to zona penetration had dissipated by the two-cell embryo stage.

The subsequent loss of the zona block to penetration is independent of ZP2 cleavage

To ascertain the relationship between ZP2 cleavage and the block to zona penetration, we used the mo$Zp2^{35-149}$/hu*ZP4* and mo$Zp2^{35-262}$/hu*ZP4* transgenic mice that contain the sperm-binding domain of ZP2. Using mAb to the N-terminus of ZP2 and immunoblots, we documented cleavage of wildtype ZP2 in the zona surrounding 2 cell embryos. The moZP2$^{35-149}$/huZP4 fusion protein lacks the ZP2 cleavage site (^{167}LA$^{\downarrow}$DE^{170}) and remains uncleaved whereas the moZP2$^{35-262}$/huZP4 fusion protein that contains the site is cleaved after fertilization (Figure 4A). Sperm bind robustly to the zona pellucida surface of eggs from each of the three genotypes but bind only to the zona matrix of two-cell embryos from mo$Zp2^{35-149}$/hu*ZP4* mice in which ZP2 cannot be cleaved (Figures 4B and 4C).

We further document that sperm binding to the zona matrix is necessary for sperm penetration of the zona pellucida after the transient block to penetration is lost. Ovulated

eggs from wildtype, mo*Zp2*$^{35-149}$/hu*ZP4* and mo*Zp2*$^{35-262}$/hu*ZP4* mice were inseminated *in vitro* with capacitated mouse sperm (5×10^5 ml^{-1}). After 6 hr of incubation, fertilized eggs contained 2 pronuclei with few supernumerary sperm in the PVS (Figure 4D). However, the ability of sperm to bind to the zona surrounding mo*Zp2*$^{35-149}$/hu*ZP4* two-cell embryos was associated with accumulation of sperm in the perivitelline space (Figure 4E). From these observations, we conclude that the cleavage status of ZP2 determines sperm-binding to the zona matrix independent of fertilization and that the block to sperm penetration of the zona matrix is transient. Thus, when sperm bind to uncleaved ZP2 in the zona pellucida surrounding two-cell embryos from the mutant mice, they can penetrate the zona matrix and accumulate in the perivitelline space.

Ovastacin enzymatic activity is required for the transient block to zona penetration

After genetic ablation of *Astl* that encodes ovastacin, mouse sperm also bind to the zona pellucida surrounding two-cell embryos despite fertilization and cortical granule exocytosis (Burkart et al., 2012). We sought to determine if a comparable loss of the zona block to penetration observed in *Zp2*^{Mut} mice was present in *Astl*^{Null} mice. Ovulated eggs, two- and four-cell embryos were isolated from wildtype and *Astl*^{Null} female mice, inseminated with capacitated sperm for 6 hr, fixed and imaged. As noted, few sperm were observed in the PVS of wildtype eggs, two- or four-cell embryos. However, 30–45 sperm were present in the PVS of eggs, two- and four-cell embryos derived from *Astl*^{Null} female mice (Figures 5A and 5B).

To determine if the effect observed with *Astl*^{Null} eggs and embryos was due to ovastacin's enzymatic activity, CRISPR/Cas9 was used to mutate the active site of the endogenous, single-copy gene to establish *Astl*^{E183A} mutant mice (Figure 5C). Genomic DNA and cDNA sequence confirmed the mutation and these mice were crossed with *Astl*^{Null} mice. The localization of mutant ovastacin^{E183A} was determined by staining fixed eggs with antibodies to ovastacin (Burkart et al., 2012) and using *lens culinaris agglutinin* (LCA-FITC) to localize cortical granules (Ducibella et al., 1988a). The images of the *Astl*^{E183A} eggs were indistinguishable from wildtype (Figure 5D) including the presence of a cortical granule free domain imposed by the meiotic spindle (Deng et al., 2003). The loss of enzymatic activity was confirmed by immunoblot which documented the inability of *Astl*^{E183A} eggs to cleave ZP2 in two-cell embryos using wildtype and *Astl*^{Null} embryos as positive and negative controls, respectively (Figure 5E). The loss of the block to zona penetration in *Astl*^{E183A} eggs and embryos was comparable to *Astl*^{Null} mice (Figures 5A and 5B). From these observations we conclude that the transient block to sperm penetration of the zona pellucida is independent of ZP2 cleavage but requires ovastacin enzymatic activity.

Zinc sparks affect sperm motility to enable the transient block to zona penetration

After fertilization, ovulated mouse eggs release zinc into the media which, using fluorescent indicators, can be dramatically imaged as 'sparks' (Kim et al., 2011). In *Astl*^{mCherry} eggs (Figure 6A) or wildtype eggs stained with LCA-FITC (Figure 5D), cortical granules were detected by confocal microscopy circumscribing 65–70% of the peripheral plasma membrane as previously reported (Ducibella et al., 1988b; Xiong et al., 2017). When stained with Fluozin-3 AM or ZincBY-1, permeant fluorescent Zn^{+2} selective indicators, to obtain single optical sections and Z-projections, much of the egg zinc co-localized with cortical

granules (Figures 6A and S3A). Zinc sparks were detected using $Astl^{mCherry}$ mice in an $Astl^{Null}$ background as a wildtype proxy. After strontium-induced activation, zona-intact eggs were continuously imaged over 2.2 hr by confocal microscopy. Several zinc sparks of decreasing magnitude were routinely observed in each egg and concomitant with each spark, there was a decrease in the ovastacin^{mCherry} signal consistent with cortical granule exocytosis (Figure 6B and movie S1).

To precisely define the temporal relationship between fertilization and zinc sparks, zona-free eggs were pre-loaded with Hoechst 33342 to detect fusion of sperm with the egg plasma membrane (Figures 6C and S3C). Following *in vitro* insemination, motile sperm were observed at the surface of the egg and, upon gamete fusion, the Hoechst dye was concentrated by binding to sperm nuclear DNA (arrow Figure 6D). The first and most pronounced zinc spark was within 2–3 min (126 ± 7.4 sec) of gamete fusion (Figure 6D and movie S2). Cortical granule localization of zinc was strikingly lost in $Astl^{Null}$ eggs and was compromised in $Astl^{E183A}$ eggs with clumping of the zinc signal in the periphery that corresponded with decreased magnitude and number of zinc sparks in zona-intact and zona-free eggs from the two mutant mouse lines (Figures S3A–S3E).

Using eggs from $Astl^{mCherry}$ mice and frame-capture of time-lapse images, we observed zinc sparks emanating from the plasma membrane overlying cortical granules with a concomitant decrease in $Astl^{mCherry}$ signal indicative of cortical granule exocytosis (Figure 6E). Ovastacin (encoded by *Astl*) is a metalloendopeptidase in which three histidine residues (H182, H186, H192) coordinately bind Zn^{+2} in the active site (E183). However, zinc sparks are observed within 2–3 min of egg activation (Figure 6D) and yet complete cleavage of ZP2 (the only known substrate for ovastacin in the extracellular zona pellucida) is not complete until 30 min after egg activation. Thus, it seems unlikely that the zinc comes from the active site of ovastacin which would abolish enzymatic activity (Wolz and Zwilling, 1989).

Nevertheless, the release of zinc from cortical granules requires the presence of native ovastacin. No zinc sparks are observed after activation of $Astl^{Null}$ eggs or in enzymatically inactive $Astl^{E183A}$ eggs which lack autolytic activity necessary to form native three-dimensional structures (Bode et al., 1992; Guevara et al., 2010). Accumulation of zinc in subcellular organelles and its release after cell activation have been reported in multiple tissues including glutamatergic neurons and pancreatic β-cells where high levels are present in synaptic vesicles (1–6 mM) and insulin granules (few-20 mM), respectively (Dodson and Steiner, 1998; Frederickson et al., 2005; Michael et al., 2006). After activation of β-cells, zinc is released from the interstices between insulin molecules upon exocytosis of insulin granules (Foster et al., 1993; Dodson and Steiner, 1998; Vinkenborg et al., 2009). Thus, although the mechanisms by which active-site independent zinc accumulates, how it is stored and released remain to be determined, these processes may relate to the presence and/or three-dimensional structure of ovastacin in cortical granules.

To investigate a potential effect of zinc on the structure of the zona pellucida that would render it impenetrable, $Astl^{Null}$ eggs were pre-incubated with 50 μM of $MgSO_4$ (control) or $ZnSO_4$ for 1 hr (significantly longer than the < 2 min duration of zinc sparks). The eggs were then transferred to 100 μl HTF and inseminated with 3×10^5 ml^{-1} capacitated sperm for

6 hr. After fixation, the eggs were imaged, and comparable numbers of sperm were observed in the PVS after exposure to $ZnSO_4$ (63.8 ± 4.0/egg, mean ± s.e.m, n = 8–9 eggs) or $MgSO_4$ (61.2 ± 4.7). Similarly, 2 mM $MgSO_4$ (negative control) or $ZnSO_4$ was microinjected into the PVS of *Astl*^{Null} eggs which were thrice washed and transferred to 100 μl HTF where they were incubated for 6 hr with 3×10^5 ml^{-1} capacitated sperm. The presence of zinc did not affect accumulation of sperm in the PVS (64.0 ± 3.1 vs. 67.0 ± 2.7/egg for control and test eggs, respectively, n = 15–20). Thus, under these experimental conditions, the presence of high levels of zinc did not perturb the zona pellucida structure to prevent sperm penetration through the extracellular matrix.

To determine if zinc could affect sperm motility, capacitated sperm were used to inseminate strontium-activated *Astl*^{Null} eggs in HTF that were already in the presence of or absence of $ZnSO_4$ and $MgSO_4$. After 6 hr incubation, eggs were fixed and imaged to quantify sperm in the PVS. HTF alone or mixed with 25–50 μM $MgSO_4$ did not affect sperm penetration. However, sperm penetration was reduced >35% in the presence of 25 μM $ZnSO_4$ and almost completely abolished with 50 μM $ZnSO_4$ (Figures 7A and 7B). Although sperm remained motile (Figure 7C) when imaged in 50 μM $ZnSO_4$ (a physiological concentration of the metal, Que et al., 2017), there was a significant decrease in the number of rapidly motile sperm and a corresponding increase in medium or slow sperm when assayed by computer assisted sperm analysis (CASA). There were smaller, albeit significant, effects on average path velocity (VAP), straight line velocity (VSL) and linearity (LIN)(Figure 7D). Taken together, we conclude that the high concentration of Zn^{+2} released during cortical granule exocytosis inhibits sperm motility and may provide the molecular basis for the transient, post-fertilization block to zona penetration.

DISCUSSION

Although millions of sperm are deposited in the lower female reproductive tract at the time of coitus, relatively few encounter ovulated eggs in the ampulla of the oviduct. After passage through a surrounding cumulus oophorus (hyaluronan interspersed with granulosa cells), capacitated sperm bind to the extracellular zona pellucida matrix which they penetrate to enter the perivitelline space and fuse with the egg plasma membrane. Within minutes, there is an effective block to polyspermy necessary for the successful onset of development (Okabe, 2013).

ZP2-cleavage model of sperm binding to the N-terminus of ZP2

MoZP2$^{35-149}$ fused to the N-terminus of huZP4 is sufficient to support mouse sperm binding on the surface of the zona matrix. Transgenic mice expressing the chimeric mouse-human protein in a *Zp2*^{Null} background are fertile, albeit with decreased fecundity. Following fertilization, the moZP2$^{35-149}$/huZP4 fusion protein, which lacks the ovastacin cleavage site, remains intact and mouse sperm bind *de novo* to two-cell embryos despite fertilization and cortical granule exocytosis. The longer moZP2$^{35-262}$/huZP4 fusion protein contains the ovastacin cleavage site (^{167}LA$^{\downarrow}$DE^{170}). It also supports sperm binding in the absence of endogenous ZP2 and transgenic mice expressing the fusion protein are fertile. However, the moZP2$^{35-262}$/huZP4 fusion protein is cleaved following fertilization and

sperm are unable to bind or penetrate the modified zona matrix. These observations are consistent with earlier studies in which we documented that the N-terminus of ZP2 is necessary for sperm binding and fertility (Baibakov et al., 2012; Avella et al., 2014). Together these results support a ZP2-cleavage model of gamete recognition in which sperm bind to the zona pellucida if ZP2 is intact, but not if it is cleaved.

Two variations of the model deserve consideration. The first is a direct model in which sperm bind to $ZP2^{35–149}$. Following fertilization, egg cortical granules exocytose ovastacin that cleaves the N-terminus of ZP2 and renders the sperm binding site non-functional. The second is an indirect model in which sperm bind to a zona domain that is physically distant from the cleaved ZP2 domain. In this model, the N-terminus of ZP2 controls taxon-specificity of gamete recognition at the distal site and the post-fertilization cleavage of ZP2 ($^{167}LA^{\downarrow}DE^{170}$) induces a conformation change of the site to prevent sperm binding. Data from gene-edited mice support the direct, rather than the indirect, binding model.

First, $Zp1^{Null}$ mice are fertile, albeit with decreased fecundity (Rankin et al., 1999), and any sperm binding domain must lie on ZP2 and/or ZP3. Second, $ZP2^{35–149}$ is necessary (Avella et al., 2014) and sufficient (this manuscript) for mouse sperm binding and fertility. Thus, C-terminal portions of ZP2 are not required for gamete recognition in mice. Third, human sperm normally do not bind to the mouse zona pellucida (Bedford, 1977). However, after *in vitro* or *in vivo* insemination of genetically engineered mice, human sperm bind and penetrate zonae pellucidae in which human ZP2, but not human ZP3, replaces endogenous mouse proteins (Baibakov et al., 2012; Avella et al., 2014). Thus, human sperm do not require ZP3 for gamete recognition. Of note, human sperm are unable to fuse with mouse eggs (Quinn, 1979; Yanagimachi, 1984; Bianchi and Wright, 2015). Fourth, $ZP2^{39–154}$ is sufficient to support taxon-specific human sperm binding independent of other zona pellucida proteins in recombinant peptide-bead binding assays (Baibakov et al., 2012; Avella et al., 2014; Avella et al., 2016). Taken together, we conclude that sperm bind directly to the N-terminus of ZP2 and its cleavage status ($^{167}LA^{\downarrow}DE^{170}$) accounts for gamete recognition before (ZP2 intact), but not after (ZP2 cleaved), fertilization.

Sperm binding to the N-terminus of ZP2 is glycan independent

Whether sperm bind to protein or glycan on the surface on the zona pellucida has remained mired in controversy despite extensive investigations of glycan-mediated gamete recognition (Yonezawa, 2014). Results of published studies vary as to the specific glycan, whether it is N- or O-linked and to which zona protein it is attached. However, these models have general and candidate-specific caveats. First, the heterogeneity of carbohydrate side chains suggests either a need for corresponding complexity of a yet-to-be-defined sperm receptor(s) or biological inactivity of non-conforming zona glycan isoforms. Second, if mouse ZP2 cleavage is prevented by mutating the cleavage site or ablating *Astl* that encodes the cleaving enzyme, sperm bind *de novo* to the zona pellucida after fertilization and cortical granule exocytosis (Gahlay et al., 2010; Burkart et al., 2012). These observations are not consistent with glycan-release models as currently formulated in which the glycan should have been removed by glycosidases exocytosed from cortical granules. Third, genetic ablation of proposed glycan attachment sites or implicated glycosyltransferases do not cause infertility

(Liu et al., 1995; Thall et al., 1995; Lowe and Marth, 2003; Shi et al., 2004; Williams et al., 2007; Gahlay et al., 2010; this manuscript). Fourth, human sperm bind and penetrate zonae containing human ZP2 in transgenic mice that do not express glycans implicated in human gamete recognition (Pang et al., 2011; Avella et al., 2014). Thus, we conclude from biochemistry and gene-edited mice that neither O- nor N-glycans are essential for sperm binding to the N-terminus of ZP2 or for fertility.

Transient block to sperm penetration of the zona pellucida

Following fertilization, an effective block to polyspermy is essential for successful development. A definitive block that prevents sperm binding arises from the post-fertilization cleavage of ZP2 (^{167}LA$^{\downarrow}$DE^{170}) as documented by loss-of and gain-of-function assays in genetically modified mice (Gahlay et al., 2010; Burkart et al., 2012; this manuscript). However, complete ZP2 cleavage takes time and there are two more immediate blocks. The first prevents supernumerary sperm already in the PVS from fusing with the egg plasma membrane. This irreversible block is independent of cortical granule exocytosis (Wolf and Hamada, 1979; Liu, 2011), but requires fusion with sperm as it can be by-passed by intracellular sperm injection (Horvath et al., 1993; Maleszewski et al., 1996). A second block, dependent on cortical granule exocytosis but independent of ZP2 cleavage, occurs within minutes of fertilization and prevents additional sperm from penetrating through the zona matrix (Inoue and Wolf, 1975; Gahlay et al., 2010).

We document that this early zona block is transient. Sperm can bind to the zona pellucida surrounding two- and four-cell embryos from *Zp2*^{Mut} and *Astl*^{Null} female mice because ZP2 remains intact. When these embryos are re-inseminated, bound sperm penetrate and accumulate *de novo* in the perivitelline space which documents the loss of the zona block. The molecular basis of the block to penetration remains incompletely understood. The requirement for ovastacin enzymatic activity suggests possible pre-fertilization processing of a yet to be determined substrate with its release during cortical granule exocytosis or the inability of the mutant ovastacin to bind zinc. The rapidity and transient nature of the block points to small molecules that diffuse away after either structurally preventing penetration or, perhaps more likely, affecting sperm motility.

Recent reports have documented zinc accumulation in growing oocytes that is released as dramatic ‘sparks’ immediately following fertilization. This release has been implicated as playing important roles in cell-cycle progression and fitness of the developing embryo (Kim et al., 2011; Que et al., 2015; Zhang et al., 2016). Our results are consistent with these earlier observations and document co-localization of zinc in cortical granules that is released upon exocytosis. It also has been reported that pre-incubation with zinc modifies the zona matrix to reduce sperm binding (Que et al., 2017), but in our sperm penetration assay using genetically modified *Zp2*^{Mut} or *Astl*^{Null} mice, pre-incubation of the zona pellucida with 50 μM zinc (or injection of 2 mM zinc into the perivitelline space) did not affect the ability of sperm to bind to the surface or penetrate through the zona matrix.

Taken together, our evidence suggests the co-existence of at least two pools of cortical granule zinc. One is bound to the active site of ovastacin and is required for the post-fertilization enzymatic activity that cleaves ZP2 in the extracellular zona pellucida. Because

ZP2 cleavage takes ~30 min to complete, zinc must persist in the active site of ovastacin for at least that long and would not be available for sparks that dissipate within 2–3 min after egg activation. The availability of a second pool is dependent on native ovastacin and is not present in the absence of ovastacin or in the presence of structurally modified ovastacin (i.e., $Astl^{E183A}$). A simple explanation would be that zinc resides in the interstices between protein molecules as described for insulin in pancreatic insulin granules (Dunn, 2005; Li, 2014) which would be released upon exocytosis to affect the forward motility of sperm and provide a transient block to zona penetration by activated sperm.

CONCLUSIONS

These experimental results support a ZP2-cleavage model of gamete recognition in which sperm do not require O- or N-linked zona glycans to bind to the N-terminus of ZP2. After zona penetration and within minutes of fertilization, egg cortical granule exudates modify the zona pellucida. First there is a rapid, transient block to sperm penetration of the zona matrix that depends on the enzymatic activity of ovastacin and is associated with zinc sparks. Subsequently, ovastacin cleaves ZP2 within 30 min of egg activation and incapacitates the sperm docking domain which provides a definitive block to polyspermy. Sperm that do not bind to the zona pellucida cannot penetrate the zona matrix nor fuse with the egg plasma membrane. In closing, we note that these studies provide insight into elements that are essential for gamete recognition, fertilization, and the post-fertilization block to polyspermy. However, they do not exclude roles for zona glycans and or other zona proteins in maximizing reproductive fitness through formation of the zona matrix and protection of the embryo as it passes down the oviduct prior to implantation.

STAR*METHODS

Detailed methods are provided in the online version of this paper and include the following:

KEY RESOURCES TABLE

CONTACT FOR REAGENT AND RESOURCE SHARING

Further information and requests for resources and reagents should be directed to and will be fulfilled by the Lead Contact, Jurrien Dean (jurrien.dean@nih.gov).

EXPERIMANTAL MODEL AND SUBJECT DETAILS

All animal studies were performed in accordance with guidelines of the Animal Care and Use Committee of the National Institutes of Health under a Division of Intramural Research, NIDDK approved animal study protocols.

METHOD DETAILS

Generation of transgenic mice—To establish transgenic mouse lines, bacterial artificial chromosome (BAC) DNA that included either mouse *Zp2* (RP23–6513) or human *ZP4* (RP11– 484B19) were transformed into SW102 bacterial cells containing the λ prophage recombineering system (Liu et al., 2003). For mo$Zp2^{35-149}$/hu*ZP4* and mo$Zp2^{35-262}$/hu*ZP4* lines, mouse genomic DNA encoding moZP2$^{35-149}$ and moZP2$^{35-262}$ were inserted in exon

1 of human *ZP4* (70 bp downstream from first ATG). To construct mo*Zp2*$^{35-149}$/hu*ZP4*, a PCR fragment containing the *galK* operon flanked by 100 bp homologous to downstream and upstream sequence from the intended insertion site of hu*ZP4* exon1 was amplified (hu*ZP4-galK* primers; Table S2) using PrimeSTAR HS DNA Polymerase (Takara Bio USA). After digestion with DpnI and electrophoresis in 0.7% agarose gel, the amplified DNA was extracted by gel purification using QIAquick Gel Extraction Kit (Qiagen). The purified PCR fragment was electroporated into the BAC containing SW102 cells and recombinants were selected by growth on minimal media with galactose. Using a clone from this step, the *galK* cassette was inserted by recombineering with a second PCR fragment (3,416 bp) encoding moZP2$^{35-149}$ protein with 100 bp arms homologous to hu*ZP4* on either side (mo*Zp2*$^{35-149}$/hu*ZP4* primers; Table S2). For moZP2$^{35-262}$, two fragments (3,027 bp and 4,084 bp) were amplified by PCR (mo*Zp2*$^{35-262}$/hu*ZP4* N-terminus and C-terminus primers; Table S2) and digested with XhoI and EcoRV for the N-terminal fragment, and EcoRV and NotI for the C-terminal fragment. Both digested fragments were inserted into pBlueScriptII SK(+) vector (Agilent). The DNA fragment, digested with XhoI and NotI, was purified using QIAquick Gel Extraction Kit and used for recombineering. Mutant clones were selected on minimal media with 2-deoxy-galactose and confirmed by PCR using gene specific primers (Table S2) and DNA sequence. In a similar recombineering strategy, 115 bp DNA encoding ZP2^{N83Q} protein was replaced with wild type genomic region using *Zp2-galK* and *Zp2*^{N83Q} primers (Table S2) to establish the mo*Zp2*^{N83Q} and mo*Zp2*$^{35-149(N83Q)}$/hu*ZP4* transgenes.

NotI and SalI fragments containing mo*Zp2*$^{35-149}$/hu*ZP4* (15.6 kb), mo*Zp2*$^{35-262}$/hu*ZP4* (19.3 kb) and mo*Zp2*$^{35-149(N83Q)}$/hu*ZP4* (15.6 kb) transgenes and NotI fragments containing *Zp2*^{N83Q} (16.1 kb) transgenes were retrieved from BAC with pl253 (Gahlay et al., 2010; Yauger et al., 2011). After gel purification, the transgenes were injected into the pronucleus of fertilized FVB/N embryos. At least two founders were established for each transgenic line and crossed into *Zp2*^{Null} and human *ZP4* transgenic mouse lines.

Generation of *Astl*^{E183A} mouse line with CRISPR/Cas9—The CRISPR sgRNA was designed using a protospacer adjacent motif (PAM) nearest to the target sequence. The sgRNA primer (Table S3) was cloned into the pUC57-sgRNA expression vector (Addgene #51132) and *in vitro* transcribed using AmpliScribe T7-Flash Transcription Kit (Lucigen). Cas9 mRNA was *in vitro* synthesized from the MLM3613 plasmid vector (Addgene #42251) using the mMESSAGE mMACHINE T7 Kit (Thermo Fisher Scientific). Both RNAs were purified using MEGAclear Transcription Clean-Up Kit (Thermo Fisher Scientific). MII eggs were collected from hormonally stimulated B6D2$_{F1}$ female mice and *in vitro* fertilization was performed in human tubal fluid (HTF) medium (Zenith Biotech) supplemented with 4 mg/ml BSA (Equitech-Bio) using sperm collected from caudal epididymides of B6D2$_{F1}$ males. 6 hr after insemination, fertilized embryos were collected. Cas9 mRNAs (100 ng/μl), sgRNA (50 ng/μl) and donor ssDNA oligonucleotides (100 ng/μl, Table S3) were mixed and injected into the cytoplasm of zygotes in M2 medium (Zenith Biotech)(Shen et al., 2014). Injected zygotes were cultured in KSOM medium (Zenith Biotech) supplemented with 3 mg/ml BSA for 12–18 hr and two-cell embryos were transferred into the oviducts of pseudopregnant ICR female mice at E0.5.

Genotyping—Tail tips of mice were lysed in 200 μl of DirectPCR Lysis Reagent (Viagen Biotech) with proteinase K (0.2 mg/ml, Thermo Fisher Scientific) at 55 °C for 2–4 hr. To inactivate proteinase K, the samples were incubated at 85 °C for 1 hr. EmeraldAmp GT PCR Master Mix (Takara Bio USA) and gene specific primers (Table S4) were used to amplify specific DNA fragments. PCR was performed with an annealing temperature of 58 °C (55 °C for mo*Zp2*) and 35 (40 for mo*Zp2*) cycles using Mastercycler Pro (Eppendorf).

Expression of transgenes—Total RNA was isolated from tissues from 10–20 wk old mice using RNeasy Mini Kit (Qiagen). Reverse transcription reactions were performed using the PrimeScript RT Reagent Kit (Takara Bio USA). Expression of normal *Zp2*, mo$Zp2^{35-149}$/hu*ZP4*, mo$Zp2^{35-262}$/hu*ZP4*, mo$Zp2^{35-149(N83Q)}$/hu*ZP4* and mo$Zp2^{N83Q}$ transgenes was detected by RT-PCR using gene-specific primer sets (Table S5). *Gapdh* was used as a loading control and for assessment of RNA integrity.

Mating, isolation of eggs and embryos—To obtain ovulated eggs and embryo, female mice were hormonally stimulated with 5 IU of equine gonadotropohin hormone (eCH) followed 46–38 hr later by 5 IU of human chorionic hormone (hCG) as previously described (Xiong et al., 2017).

Microscopy—Images of eggs and embryos were obtained with a confocal microscope (LSM 710; Carl Zeiss). Images of ovarian sections were obtained with an inverted microscope (Axioplan 2; Carl Zeiss)(Baibakov et al., 2007; Yauger et al., 2011). LSM 710 images were exported as full resolution TIF files and processed in Photoshop CC 2017 (Adobe) to adjust brightness and contrast. Alternatively, confocal optical sections were projected to a single plane with maximum intensity and combined with differential interference contrast (DIC) images using LSM image software.

Ovarian histology and immunohistochemistry—Mouse ovaries were fixed in 3% glutaraldehyde and embedded in glycol methacrylate before staining with periodic Shiff's acid and hematoxylin (Yauger et al., 2011). Ovulated eggs were fixed in 3% paraformaldehyde for 30 min and washed in phosphate-buffered saline (PBS, Invitrogen) with 0.3 % polyvinylpyrrolidone (PVP). Eggs were incubated in PBS with 0.3% BSA (Calbiochem) and 0.1% Tween 20 for 2 hr and stained with rat or mouse monoclonal antibodies (1:500) specific to ZP1 (M1.4, Rankin et al., 1999), N-terminus of ZP2 (IE-3, East and Dean, 1984), C-terminus of ZP2 (m2c.2, Rankin et al., 2003), ZP3 (IE-10, East et al., 1985) and huZP4 (1:200, Bukovsky et al., 2008). Monoclonal antibodies to human ZP4 were a gift from S. Gupta (National Institute of Immunology, New Delhi, India). For secondary antibodies, goat anti-mouse antibody conjugated with Alexa Fluor 488 (1:500, Invitrogen) or goat anti-rat antibody conjugated with Alexa Fluor 488 (1:500, Invitrogen) were used.

N-glycosidase treatment of zonae pellucidae—Deglycosylation was performed according to the manufacturer's instructions (New England Biolabs). 15 eggs were added in 10 μl of 1X glycoprotein denaturing buffer, heated at 100 °C for 10 min, chilled on ice for 1 min, centrifuged and supernatants were decanted. The pellet was resuspended in 2 μl 10X

Glyco buffer 2, 2 μl 10% NP-40, 5 μl H_2O and 1 μl PNGase F. Samples were incubated at 37 °C for 4 hr.

Immunoblot—Ovulated eggs were collected from hormonally stimulated female mice and cumulus cells were removed by hyaluronidase (1 mg/ml, <5 min at 37 °C). 10–30 eggs or two-cell embryos were lysed in LDS sample buffer (Invitrogen) or Tris-Glycine SDS sample buffer (Invitrogen) with 5% 2-mercaptoethanol. Samples were separated on 4–12% Bis-Tris gels or 4–20% Tris-Glycine gels by SDS-PAGE and transferred to polyvinylidene fluoride membranes (Bio-Rad). Membranes were blocked in 5% nonfat milk (BD Biosciences) in Tris-buffered saline (TBS) with 0.05% Tween-20 (Takara Bio USA) and probed with primary antibodies to the N-terminus or C-terminus of ZP2, ZP3 and α-tubulin (MBL) followed by secondary antibodies conjugated to HRP (Jackson ImmunoReserch Laboratories). Chemiluminescence reactions were performed with ECL Prime (GE Healthcare) and signals were detected using PXi Touch (SYNGENE) or Hyperfilm ECL (GE Healthcare) according to the manufacturers' instructions.

Assessment of sperm binding and penetration—To assay mouse sperm binding to the zona pellucida surrounding normal and transgenic mouse eggs and embryos, sperm were collected from the cauda epididymides of $B6D2_{F1}$ male mice and pre-incubated in HTF medium supplemented with 4 mg/ml BSA for 1.5 hr. Capacitated sperm were added to cumulus-free eggs and embryos in 500 μl of HTF medium at a final concentration of 2×10^5 ml^{-1}. After incubation for 30 min, samples were washed with a wide-bore pipette to remove loosely adherent sperm using $ZP3^{EGFP}$ mouse eggs and two-cell embryos as positive and negative controls, respectively. Samples were fixed in 3% paraformaldehyde and stained with Hoechst 33342 dye to visualize nuclei. The number of bound sperm was quantified from z-projections obtained by confocal microscopy (Baibakov et al., 2007) and the results reflect the mean ± s.e.m. from at least three independently obtained samples.

Ovulated eggs from wildtype and transgenic mice were treated with hyaluronidase to remove cumulus and placed in HTF media. Eggs were either activated by treatment with 10 mM $SrCl_2$ (Kline and Kline, 1992) or fertilized with epididymal myristoylated EGFP sperm (Lin et al., 2014). Fertilized eggs were transferred to KSOM medium and incubated for 16 and 40 hr, respectively, to obtain two- and four-cell embryos. Capacitated sperm from $B6D2_{F1}$ mice were added to 100 μl HTF medium containing MII eggs, strontium-activated eggs, two- or four-cell embryos at a final concentration of 5×10^5 ml^{-1} (wildtype, mo$Zp2^{35-149}$/hu*ZP4*, mo$Zp2^{35-262}$/hu*ZP4* and mo$Zp2^{35-149(N83Q)}$/hu*ZP4*) or 3×10^5 ml^{-1} (mo$Zp2^{Mut}$, $Astl^{Null}$ and $Astl^{E183A}$). After incubation for 6 hr, loosely adherent sperm were removed by pipetting and eggs/embryos were fixed in 3% paraformaldehyde. Zona pellucida and nuclei were stained with wheat germ agglutinin (WGA) conjugated Alexa 633 and Hoechst 33342, respectively.

***In vitro* and *in vivo* fertility assays—**To assess *in vitro* fertility, ovulated eggs were collected from hormonally stimulated female mice. Capacitated sperm collected from $B6D2_{F1}$ male mice were added in 100 μl HTF medium with cumulus-intact or cumulus-free eggs at a final concentration 5×10^5 ml^{-1}. After incubation for 6 hr, fertilized eggs were evaluated by formation of two pronuclei.

To assess *in vivo* fertility, hormonally stimulated females were co-caged with $B6D2_{F1}$ males. 22–24 hr after hCG injection, eggs were collected from the oviducts of female mice with copulation plugs, and fertilized eggs were scored by formation of two pronuclei. To examine litter sizes, females (≥5) from each mouse line were singly co-caged with a fertile female (control) and mated (2:1) with a male proven to be fertile. Litters were recorded until the control female gave birth to at least three litters or after 5 months of mating.

Effect of zinc on zona penetration and sperm motility—Sperm were collected from cauda epididymides of $B6D2_{F1}$ mice, capacitated in HTF medium supplemented with 4 mg/ml BSA for 1.5 hr. To assay the effect of Zn^{2+} on zonae pellucidae, $Astl^{Null}$ eggs were collected, treated with hyaluronidase and pre-incubated in HTF medium supplemented with 50 μM $MgSO_4$ or $ZnSO_4$ for 1 hr. Alternatively, to mimic zinc sparks released from eggs, M2 medium with 2 mM of $MgSO_4$ or $ZnSO_4$ was injected into the perivitelline space of $Astl^{Null}$ eggs using a FemtoJet 4i (Eppendorf) until the zona pellucida was swollen. Under each experimental condition, eggs were then thrice washed in 30 μl droplets of HTF medium, inseminated with capacitated sperm (3×10^5 ml^{-1} final concentration) in 100 μl of HTF and incubated for 6 hr. To determine the effect of Zn^{2+} on mouse sperm motility, Capacitated sperm were added in 100 μl of HTF with 25–50 μM $MgSO_4$ or $ZnSO_4$ at a final concentration of 5×10^5 ml^{-1}. Sperm motility were determined by a HTM-IVOS (Version 12.3) motility analyzer (Hamilton Thorne).

Imaging zinc localization in eggs and zinc sparks—To observe zinc localization in MII eggs, cumulus-free eggs were incubated in HTF medium with 50 nM ZincBY-1 or FluoZin-3 AM for 15 min (Que et al., 2015). Eggs were imaged in 200 μl drops of M2 medium on glass-bottom dishes (MatTek Corporation) covered with liquid paraffin (Nacalai Tesque).

To observe zinc sparks after strontium-induced activation, cumulus-free eggs were allowed to settle in a 40 μl drop of Ca^{2+} and Mg^{2+}-free HTF medium on a glass-bottom dish coated with poly-L-lysine. After 10 min, 10 μl Ca^{2+} and Mg^{2+}-free HTF medium containing 4 mg/ml BSA, 50 mM $SrCl_2$ and 500 μM FluoZin-3, tetrapotassium salt (Invitrogen) was slowly added (Kim et al., 2011). The dish was placed in a humidified chamber (5% CO_2, 37 °C) attached to the microscope. To observe zinc sparks after fertilization of zona-intact MII eggs, capacitated sperm were added at a final concentration 1×10^5 ml^{-1}. Alternatively, zonae pellucidae were removed by treatment with Tyrode's solution (Sigma Aldrich). Zona-free eggs were preloaded with Hoechst 33342 and allowed to settle in a 30 μl drop of HTF medium without BSA on a glass-bottom dish coated with poly-L-lysine prior to insemination. The mCherry signal was excited with a 561-nm laser line and detected with a 575–615-nm band pass. The zinc indicator signal was excited with a 488-nm laser line and detected with a 500–560-nm band pass. Image acquisition began immediately, and images were taken every 3 sec for a total 9000 sec (2.5 hr) or every 4 sec for a total 8000 sec (2.2 hr).

QUANTIFICATION AND STATISTICAL ANALYSIS

The two-tailed Student's t-test was used to calculate P values. Statistically significant values for $P < 0.05$, $P < 0.005$ and $P < 0.001$ are indicated by single, double, and triple asterisks, respectively.

Supplementary Material

Refer to Web version on PubMed Central for supplementary material.

ACKNOWLEDGEMENTS

We thank Dr. Boris Baibakov for help with confocal microscopy and all the members of J.D.'s laboratory for helpful suggestions on the project. This research was supported by the Intramural Research Program of the NIH, The National Institute of Diabetes and Digestive and Kidney Disease (NIDDK). K.T. was supported by fellowship grants from the Uehara Memorial Foundation, Kanae Foundation for the Promotion of Medical Science and the Japan Society for the Promotion of Science.

REFERENCES

Abou-Haila A, Bendahmane M, and Tulsiani DR (2014). Significance of egg's zona pellucida glycoproteins in sperm-egg interaction and fertilization. Minerva Ginecol 66, 409–419. [PubMed: 25020059]

Avella MA, Baibakov B, and Dean J (2014). A single domain of the ZP2 zona pellucida protein mediates gamete recognition in mice and humans. J Cell Biol 205, 801–809. [PubMed: 24934154]

Avella MA, Baibakov B, Jimenez-Movilla M, Sadusky AB, and Dean J (2016). ZP2 peptide-beads select human sperm in vitro, decoy mouse sperm in vivo and provide reversible contraception. Sci Transl Med 8, 336ra360.

Avella MA, Xiong B, and Dean J (2013). The molecular basis of gamete recognition in mice and humans. Mol Hum Reprod 19, 279–289. [PubMed: 23335731]

Baibakov B, Boggs NA, Yauger B, Baibakov G, and Dean J (2012). Human sperm bind to the N-terminal domain of ZP2 in humanized zonae pellucidae in transgenic mice. J Cell Biol 197, 897–905. [PubMed: 22734000]

Baibakov B, Gauthier L, Talbot P, Rankin TL, and Dean J (2007). Sperm binding to the zona pellucida is not sufficient to induce acrosome exocytosis. Development 134, 933–943. [PubMed: 17293534]

Bauskin AR, Franken DR, Eberspaecher U, and Donner P (1999). Characterization of human zona pellucida glycoproteins. Mol Hum Reprod 5, 534–540. [PubMed: 10341000]

Bedford JM (1977). Sperm/egg interaction: The specificity of human spermatozoa. Anat Rec 188, 477–488. [PubMed: 409311]

Bianchi E, and Wright GJ (2015). Cross-species fertilization: the hamster egg receptor, Juno, binds the human sperm ligand, Izumo1. Philos Trans R Soc Lond B Biol Sci 370, 20140101. [PubMed: 25533103]

Bleil JD, and Wassarman PM (1980a). Mammalian sperm-egg interaction: Identification of a glycoprotein in mouse egg zonae pellucidae possessing receptor activity for sperm. Cell 20, 873–882. [PubMed: 7418009]

Bleil JD, and Wassarman PM (1980b). Structure and function of the zona pellucida: Identification and characterization of the proteins of the mouse oocyte's zona pellucida. Dev Biol 76, 185–202. [PubMed: 7380091]

Bode W, Gomis-Ruth FX, Huber R, Zwilling R, and Stocker W (1992). Structure of astacin and implications for activation of astacins and zinc-ligation of collagenases. Nature 358, 164–167. [PubMed: 1319561]

Boja ES, Hoodbhoy T, Fales HM, and Dean J (2003). Structural characterization of native mouse zona pellucida proteins using mass spectrometry. J Biol Chem 278, 34189–34202. [PubMed: 12799386]

Bukovsky A, Gupta SK, Bansal P, Chakravarty S, Chaudhary M, Svetlikova M, White RS, Copas P, Upadhyaya NB, Van Meter SE, et al. (2008). Production of monoclonal antibodies against recombinant human zona pellucida glycoproteins: utility in immunolocalization of respective zona proteins in ovarian follicles. J Reprod Immunol 78, 102–114. [PubMed: 18313762]

Burkart AD, Xiong B, Baibakov B, Jimenez-Movilla M, and Dean J (2012). Ovastacin, a cortical granule protease, cleaves ZP2 in the zona pellucida to prevent polyspermy. J Cell Biol 197, 37–44. [PubMed: 22472438]

Chiu PC, Lam KK, Wong RC, and Yeung WS (2014). The identity of zona pellucida receptor on spermatozoa: an unresolved issue in developmental biology. Semin Cell Dev Biol 30, 86–95. [PubMed: 24747367]

Clark GF (2014). A role for carbohydrate recognition in mammalian sperm-egg binding. Biochem Biophys Res Commun 450, 1195–1203. [PubMed: 24952156]

Deng M, Kishikawa H, Yanagimachi R, Kopf GS, Schultz RM, and Williams CJ (2003). Chromatin-mediated cortical granule redistribution is responsible for the formation of the cortical granule-free domain in mouse eggs. Dev Biol 257, 166–176. [PubMed: 12710965]

Dodson G, and Steiner D (1998). The role of assembly in insulin's biosynthesis. Curr Opin Struct Biol 8, 189–194. [PubMed: 9631292]

Ducibella T, Anderson E, Albertini DF, Aalberg J, and Rangarajan S (1988a). Quantitative studies of changes in cortical granule number and distribution in the mouse oocyte during meiotic maturation. Dev Biol 130, 184–197. [PubMed: 3141231]

Ducibella T, Rangarajan S, and Anderson E (1988b). The development of mouse oocyte cortical reaction competence is accompanied by major changes in cortical vesicles and not cortical granule depth. Dev Biol 130, 789–792. [PubMed: 3197932]

Dunn MF (2005). Zinc-ligand interactions modulate assembly and stability of the insulin hexamer -- a review. BioMetals 18, 295–303. [PubMed: 16158220]

East IJ, and Dean J (1984). Monoclonal antibodies as probes of the distribution of ZP-2, the major sulfated glycoprotein of the murine zona pellucida. J Cell Biol 98, 795–800. [PubMed: 6699085]

East IJ, Gulyas BJ, and Dean J (1985). Monoclonal antibodies to the murine zona pellucida protein with sperm receptor activity: Effects on fertilization and early development. Dev Biol 109, 268–273. [PubMed: 3996750]

Foster MC, Leapman RD, Li MX, and Atwater I (1993). Elemental composition of secretory granules in pancreatic islets of Langerhans. Biophys J 64, 525–532. [PubMed: 8457676]

Frederickson CJ, Koh JY, and Bush AI (2005). The neurobiology of zinc in health and disease. Nat Rev Neurosci 6, 449–462. [PubMed: 15891778]

Gahlay G, Gauthier L, Baibakov B, Epifano O, and Dean J (2010). Gamete recognition in mice depends on the cleavage status of an egg's zona pellucida protein. Science 329, 216–219. [PubMed: 20616279]

Guevara T, Yiallouros I, Kappelhoff R, Bissdorf S, Stocker W, and Gomis-Ruth FX (2010). Proenzyme structure and activation of astacin metallopeptidase. J Biol Chem 285, 13958–13965. [PubMed: 20202938]

Horvath PM, Kellom T, Caulfield J, and Boldt J (1993). Mechanistic studies of the plasma membrane block to polyspermy in mouse eggs. Mol Reprod Dev 34, 65–72. [PubMed: 8418819]

Hwang WY, Fu Y, Reyon D, Maeder ML, Tsai SQ, Sander JD, Peterson RT, Yeh JR, and Joung JK (2013). Efficient genome editing in zebrafish using a CRISPR-Cas system. Nat Biotechnol 31, 227–229. [PubMed: 23360964]

Inoue M, and Wolf DP (1975). Sperm binding characteristics of the murine zona pellucida. Biol Reprod 13, 340–346. [PubMed: 1218199]

Kim AM, Bernhardt ML, Kong BY, Ahn RW, Vogt S, Woodruff TK, and O'Halloran TV (2011). Zinc sparks are triggered by fertilization and facilitate cell cycle resumption in mammalian eggs. ACS Chem Biol 6, 716–723. [PubMed: 21526836]

Kline D, and Kline JT (1992). Repetitive calcium transients and the role of calcium in exocytosis and cell cycle activation in the mouse egg. Dev Biol 149, 80–89. [PubMed: 1728596]

Lefièvre L, Conner SJ, Salpekar A, Olufowobi O, Ashton P, Pavlovic B, Lenton W, Afnan M, Brewis IA, Monk M, et al. (2004). Four zona pellucida glycoproteins are expressed in the human. Hum Reprod 19, 1580–1586. [PubMed: 15142998]

Li YV (2014). Zinc and insulin in pancreatic beta-cells. Endocrine 45, 178–189. [PubMed: 23979673]

Lin RS, Jimenez-Movilla M, and Dean J (2014). Figla-Cre transgenic mice expressing myristoylated EGFP in germ cells provide a model for investigating perinatal oocyte dynamics. PLoS One 9, e84477. [PubMed: 24400092]

Liu C, Litscher ES, Mortillo S, Sakai Y, Kinloch RA, Stewart CL, and Wassarman PM (1996). Targeted disruption of the *mZP3* gene results in production of eggs lacking a zona pellucida and infertility in female mice. Proc Natl Acad Sci U S A 93, 5431–5436. [PubMed: 8643592]

Liu C, Litscher S, and Wassarman PM (1995). Transgenic mice with reduced numbers of functional sperm receptors on their eggs reproduce normally. Mol Biol Cell 6, 577–585. [PubMed: 7663023]

Liu M (2011). The biology and dynamics of mammalian cortical granules. Reprod Biol Endocrinol 9, 149. [PubMed: 22088197]

Liu P, Jenkins NA, and Copeland NG (2003). A highly efficient recombineering-based method for generating conditional knockout mutations. Genome Res 13, 476–484. [PubMed: 12618378]

Lowe JB, and Marth JD (2003). A genetic approach to mammalian glycan function. Annu Rev Biochem 72, 643–691. [PubMed: 12676797]

Maleszewski M, Kimura Y, and Yanagimachi R (1996). Sperm membrane incorporation into oolemma contributes to the oolemma block to sperm penetration: evidence based on intracytoplasmic sperm injection experiments in the mouse. Mol Reprod Dev 44, 256–259. [PubMed: 9115725]

Michael DJ, Ritzel RA, Haataja L, and Chow RH (2006). Pancreatic beta-cells secrete insulin in fast- and slow-release forms. Diabetes 55, 600–607. [PubMed: 16505221]

Okabe M (2013). The cell biology of mammalian fertilization. Development 140, 4471–4479. [PubMed: 24194470]

Pang PC, Chiu PC, Lee CL, Chang LY, Panico M, Morris HR, Haslam SM, Khoo KH, Clark GF, Yeung WS, et al. (2011). Human sperm binding is mediated by the sialyl-Lewis(x) oligosaccharide on the zona pellucida. Science 333, 1761–1764. [PubMed: 21852454]

Que EL, Bleher R, Duncan FE, Kong BY, Gleber SC, Vogt S, Chen S, Garwin SA, Bayer AR, Dravid VP, et al. (2015). Quantitative mapping of zinc fluxes in the mammalian egg reveals the origin of fertilization-induced zinc sparks. Nat Chem 7, 130–139. [PubMed: 25615666]

Que EL, Duncan FE, Bayer AR, Philips SJ, Roth EW, Bleher R, Gleber SC, Vogt S, Woodruff TK, and O'Halloran TV (2017). Zinc sparks induce physiochemical changes in the egg zona pellucida that prevent polyspermy. Integr Biol (Camb) 9, 135–144. [PubMed: 28102396]

Quesada V, Sanchez LM, Alvarez J, and Lopez-Otin C (2004). Identification and characterization of human and mouse ovastacin: a novel metalloproteinase similar to hatching enzymes from arthropods, birds, amphibians, and fish. J Biol Chem 279, 26627–26634. [PubMed: 15087446]

Quinn P (1979). Failure of human spermatozoa to penetrate zona free mouse and rat ova in vitro. J Exp Zool 210, 497–505. [PubMed: 541604]

Rankin T, Familari M, Lee E, Ginsberg AM, Dwyer N, Blanchette-Mackie J, Drago J, Westphal H, and Dean J (1996). Mice homozygous for an insertional mutation in the *Zp3* gene lack a zona pellucida and are infertile. Development 122, 2903–2910. [PubMed: 8787763]

Rankin T, Talbot P, Lee E, and Dean J (1999). Abnormal zonae pellucidae in mice lacking ZP1 result in early embryonic loss. Development 126, 3847–3855. [PubMed: 10433913]

Rankin TL, Coleman JS, Epifano O, Hoodbhoy T, Turner SG, Castle PE, Lee E, Gore-Langton R, and Dean J (2003). Fertility and taxon-specific sperm binding persist after replacement of mouse 'sperm receptors' with human homologues. Dev Cell 5, 33–43. [PubMed: 12852850]

Rankin TL, O'Brien M, Lee E, Wigglesworth KE, J.J., and Dean J (2001). Defective zonae pellucidae in *Zp2* null mice disrupt folliculogenesis, fertility and development. Development 128, 1119–1126. [PubMed: 11245577]

Shen B, Zhang W, Zhang J, Zhou J, Wang J, Chen L, Wang L, Hodgkins A, Iyer V, Huang X, et al. (2014). Efficient genome modification by CRISPR-Cas9 nickase with minimal off-target effects. Nat Methods 11, 399–402. [PubMed: 24584192]

Shi S, Williams SA, Seppo A, Kurniawan H, Chen W, Zhengyi Y, Marth JD, and Stanley P (2004). Inactivation of the *MgatI* gene in oocytes impairs oogenesis, but embryos lacking complex and hybrid N-glycans develop and implant. Mol Cell Biol 24, 9920–9929. [PubMed: 15509794]

Thall AD, Maly P, and Lowe JB (1995). Oocyte gal alpha 1,3gal epitopes implicated in sperm adhesion to the zona pellucida glycoprotein ZP3 are not required for fertilization in the mouse. J Biol Chem 270, 21437–21440. [PubMed: 7545161]

Tian J, Gong H, Thomsen GH, and Lennarz WJ (1997). Gamete interactions in *Xenopus laevis*: Identification of sperm binding glycoproteins in the egg vitelline envelope. J Cell Biol 136, 1099–1108. [PubMed: 9060474]

Vinkenborg JL, Nicolson TJ, Bellomo EA, Koay MS, Rutter GA, and Merkx M (2009). Genetically encoded FRET sensors to monitor intracellular Zn2+ homeostasis. Nat Methods 6, 737–740. [PubMed: 19718032]

Warming S, Costantino N, DL C, Jenkins NA, and Copeland NG (2005). Simple and highly efficient BAC recombineering using galK selection. Nucleic Acids Res 33, e36. [PubMed: 15731329]

Williams SA, Xia L, Cummings RD, McEver RP, and Stanley P (2007). Fertilization in the mouse does not require terminal galactose or N-acetylglucosamine on the zona pellucida glycans. J Cell Sci 120, 1341–1349. [PubMed: 17374637]

Wolf DP, and Hamada M (1979). Sperm binding to the mouse egg plasmalemma. Biol Reprod 21, 205–211. [PubMed: 486637]

Wolz RL, and Zwilling R (1989). Kinetic evidence for cooperative binding of two ortho-phenanthroline molecules to astacus protease during metal removal. J Inorg Biochem 35, 157–167. [PubMed: 2723627]

Wong JL, and Wessel GM (2006). Defending the zygote: search for the ancestral animal block to polyspermy. Curr Top Dev Biol 72, 1–151. [PubMed: 16564333]

Xiong B, Zhao Y, Beall S, Sadusky AB, and Dean J (2017). A unique egg cortical granule localization motif is required for ovastacin sequestration to prevent premature ZP2 cleavage and ensure female fertility in mice. PLoS Genet 13, e1006580. [PubMed: 28114310]

Yanagimachi R (1984). Zona-free hamster eggs: Their use in assessing fertilizing capacity and examining chromosomes of human spermatozoa. Gamete Res 10, 187–232.

Yanagimachi R (1994). Mammalian fertilization In The Physiology of Reproduction, Knobil E, and Neil J, eds. (New York: Raven Press), pp. 189–317.

Yauger B, Boggs N, and Dean J (2011). Human ZP4 is not sufficient for taxon-specific sperm binding to the zona pellucida in transgenic mice. Reproduction 141, 313–319. [PubMed: 21173071]

Yonezawa N (2014). Posttranslational modifications of zona pellucida proteins. Adv Exp Med Biol 759, 111–140. [PubMed: 25030762]

Zhang N, Duncan FE, Que EL, O'Halloran TV, and Woodruff TK (2016). The fertilization-induced zinc spark is a novel biomarker of mouse embryo quality and early development. Sci Rep 6, 22772. [PubMed: 26987302]

Zhao M, Gold L, Ginsberg AM, Liang L-F, and Dean J (2002). Conserved furin cleavage site not essential for secretion and integration of ZP3 into the extracellular egg coat of transgenic mice. Mol Cell Biol 22, 3111–3120. [PubMed: 11940668]

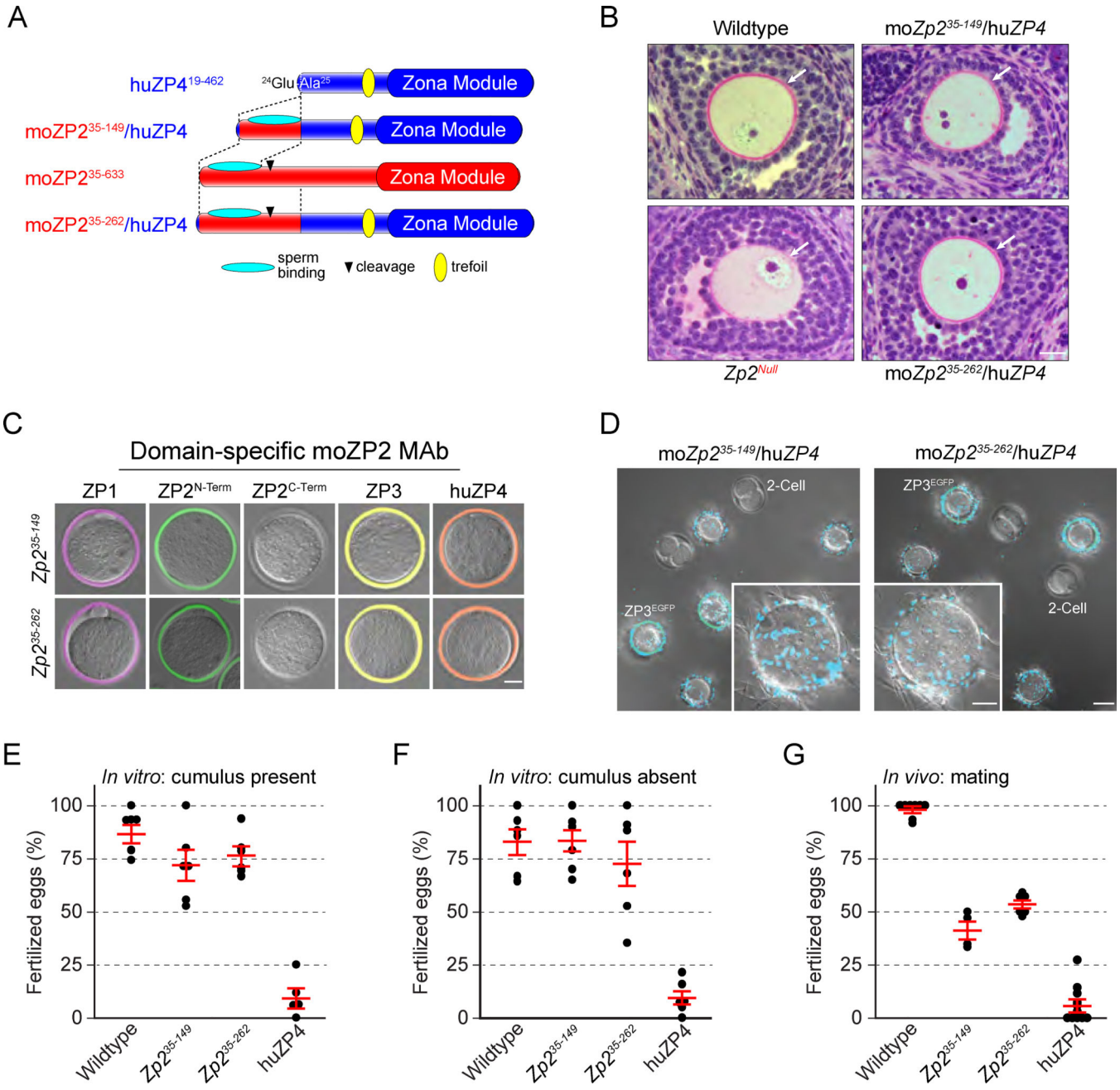

Figure 1. The N-terminus of ZP2 is sufficient for sperm binding and fertility

(A) Schematic representation of huZP4, moZP2, chimeric moZP2$^{35-149}$/huZP4, and moZP2$^{35-262}$/huZP4 fusion proteins. Blue and red bar represents huZP4 and moZP2 proteins, respectively. Green oval, sperm binding site. Inverted triangle, ^{167}LA$^{\downarrow}$DE^{170} cleavage site. Yellow oval, trefoil domain.

(B) Wildtype, *Zp2*^{Null}, mo*Zp2*$^{35-149}$/hu*ZP4* and mo*Zp2*$^{35-262}$/hu*ZP4* rescue ovaries were fixed in glutaraldehyde, embedded in plastic, sectioned, stained with PAS to high-light the extracellular zona pellucida (arrow) and imaged. Scale bar, 20 μm.

(C) Confocal images of unfertilized eggs from mo*Zp2*$^{35-149}$/hu*ZP4* and mo*Zp2*$^{35-262}$/hu*ZP4* rescue mice using antibodies to: moZP1 (M1.4), moZP2$^{\text{N-term}}$ (IE-3), moZP2$^{\text{C-term}}$ (m2c.2), moZP3 (IE-10) and huZP4 (Bukovsky et al., 2008). Chimeric proteins derived from each transgene were incorporated into the zona matrix. Scale bar, 20 μm.

(D) Sperm binding to unfertilized moZP2$^{35-149}$/huZP4 and moZP2$^{35-262}$/huZP4 rescue eggs. ZP3$^{\text{EGFP}}$ eggs and two-cell embryos were used as positive and negative wash controls, respectively. Scale bar, 50 μm and 20 μm (inset).

(E) *In vitro* fertility (2 pronuclei) of wildtype, moZP2$^{35-149}$/huZP4, moZP2$^{35-262}$/huZP4 and huZP4 rescue eggs (red bars, mean ± s.e.m.) in cumulus after insemination with capacitated epididymal mouse sperm (5×10^5 ml^{-1}).

(F) Same as (E), but after removal of the cumulus mass by hyaluronidase.

(G) *In vivo* fertility (2 pronuclei) of wildtype, moZP2$^{35-149}$/huZP4, moZP2$^{35-262}$/huZP4 and huZP4 rescue eggs (red bars, mean ± s.e.m.). Female mice were hormonally stimulated, mated with males proven to be fertile and egg/zygotes were isolated from oviducts 22 hr after administration of hCG.

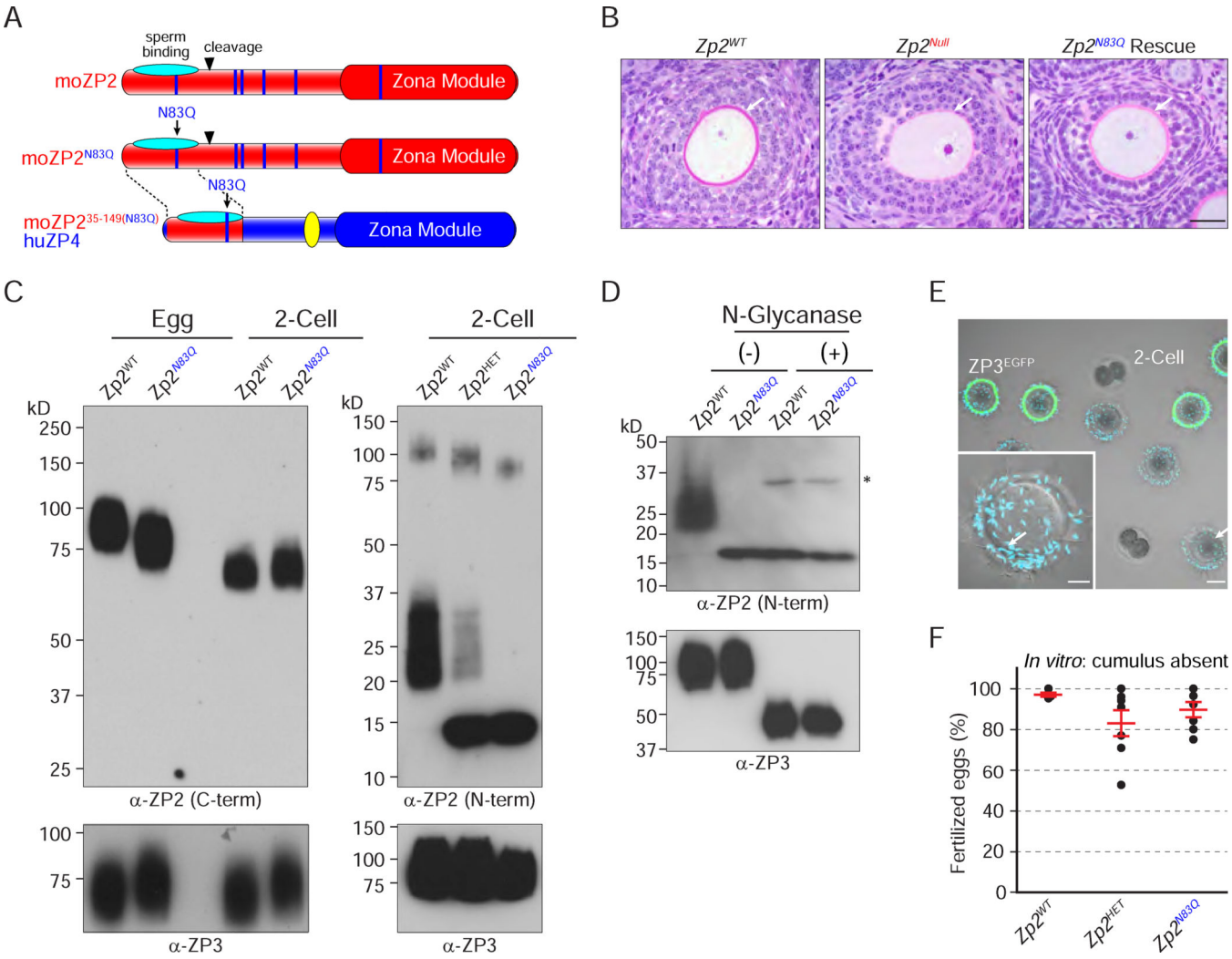

Figure 2. The N-glycan at the N-terminus of ZP2 is not essential for sperm binding and fertility

(A) Schematics of secreted ZP2$^{35-633}$ with N-terminal sperm binding domain and C-terminal zona module, mutant ZP2^{N83Q} and mutant ZP2$^{35-149(N83Q)}$/ZP4 fusion protein. Blue and red bar represents huZP4 and moZP2 proteins, respectively. Vertical blue bars represent the six N-glycans (N83, N172, N184, N217, N264, N393) attachment sites. Arrow, ZP2^{N83Q} mutation. Inverted triangle, ^{167}LA$^{\downarrow}$DE^{170} cleavage site. Yellow oval, trefoil domain.

(B) Ovaries from wildtype, *Zp2^{Null}*, and *Zp2^{N83Q}* rescue mice were fixed in glutaraldehyde, embedded in plastic, sectioned, stained with PAS and imaged. Arrows, zona pellucida. Scale bar, 40 μm.

(C) Immunoblot of wildtype, ZP2^{N83Q} rescue zonae pellucidae using monoclonal antibodies to ZP2$^{C\text{-term}}$ (upper, left), ZP2$^{N\text{-term}}$ (upper, right) and ZP3 (lower). Ovulated eggs (10/lane) were obtained after hormonal stimulation and two-cell embryos [10 (left) or 20 (right)/lane] were obtained after *in vivo* mating.

(D) Immunoblot of wildtype and ZP2^{N83Q} rescue eggs before and treatment with PNGase F using monoclonal antibodies to ZP2$^{N\text{-term}}$ (upper) and ZP3 (lower). Asterisk, N-glycanase.

(E) Sperm binding to $Zp2^{N83Q}$ rescue eggs using $Zp3^{EGFP}$ eggs and two-cell embryos as positive and negative wash controls, respectively. Scale bar, 50 μm and 20 μm (inset).
(F) *In vitro* fertilization (red bars, mean ± s.e.m.) of wildtype, hetero- and homozygous $Zp2^{N83Q}$ rescue eggs after removal of cumulus mass by hyaluronidase treatment.

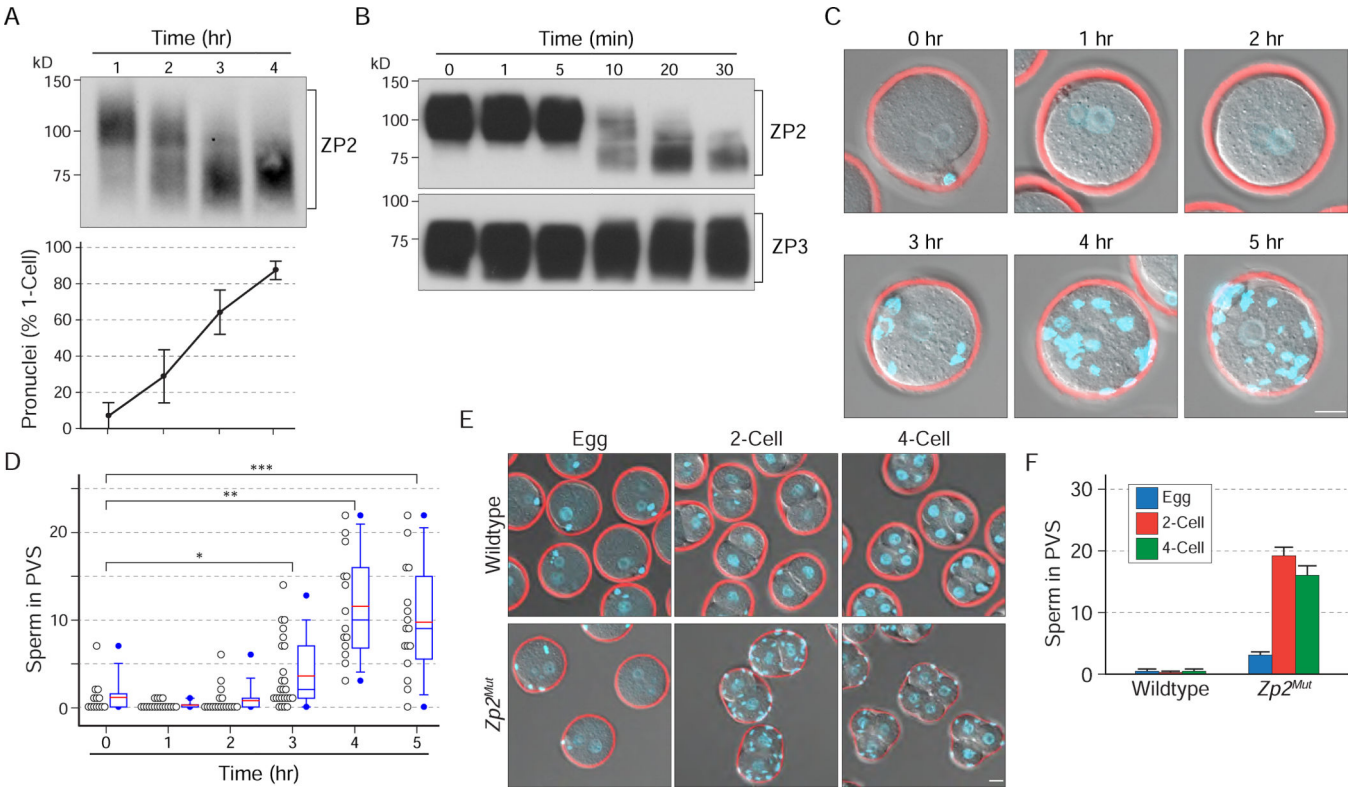

Figure 3. Establishing the transient block to sperm penetration of the zona pellucida

(A) Cleavage of ZP2 (upper) and fertility (2 pronuclei, mean ± s.e.m., lower) after *in vitro* fertilization with capacitated sperm (5×10^5 ml^{-1}). Representative immunoblot documents ZP2 cleavage beginning 2 hr after insemination.

(B) Immunoblot of ZP2 with monoclonal antibodies to $ZP2^{C\text{-}term}$ (upper) and ZP3 (lower) over time after egg activation with $SrCl_2$.

(C) After treatment with $SrCl_2$ to activate $Zp2^{Mut}$ eggs, *in vitro* insemination with capacitated epididymal sperm was delayed 0–5 hr. Fertilized eggs were then incubated for an additional 6 hr, fixed, stained with Hoechst and WGA conjugated Alexa Flour 633 prior to imaging to determine the number of supernumerary sperm in the perivitelline space (PVS). Scale bar, 20 μm.

(D) Quantification of the number of sperm in the PVS in (C). For each time point, a dot density plot is on the left and a box plot is on the right. The boundary of the box closest to zero indicates the 25th percentile, a line within the box marks the median, a red line marks the mean, and the boundary of the box farthest from zero indicates the 75th percentile. Error bars above and below the box indicate the 90th and 10th percentiles and the dots are outliers. The 2-tailed Student's t-test determined statistical differences, *** P <0.001, ** P <0.005, * P <0.05.

(E) Images of sperm in the PVS after insemination of wildtype and $Zp2^{Mut}$ rescue eggs, two- and four-cell embryos. Scale bar, 20 μm.

(F) Quantification of the number of sperm in the PVS (mean ± s.e.m.) in (E).

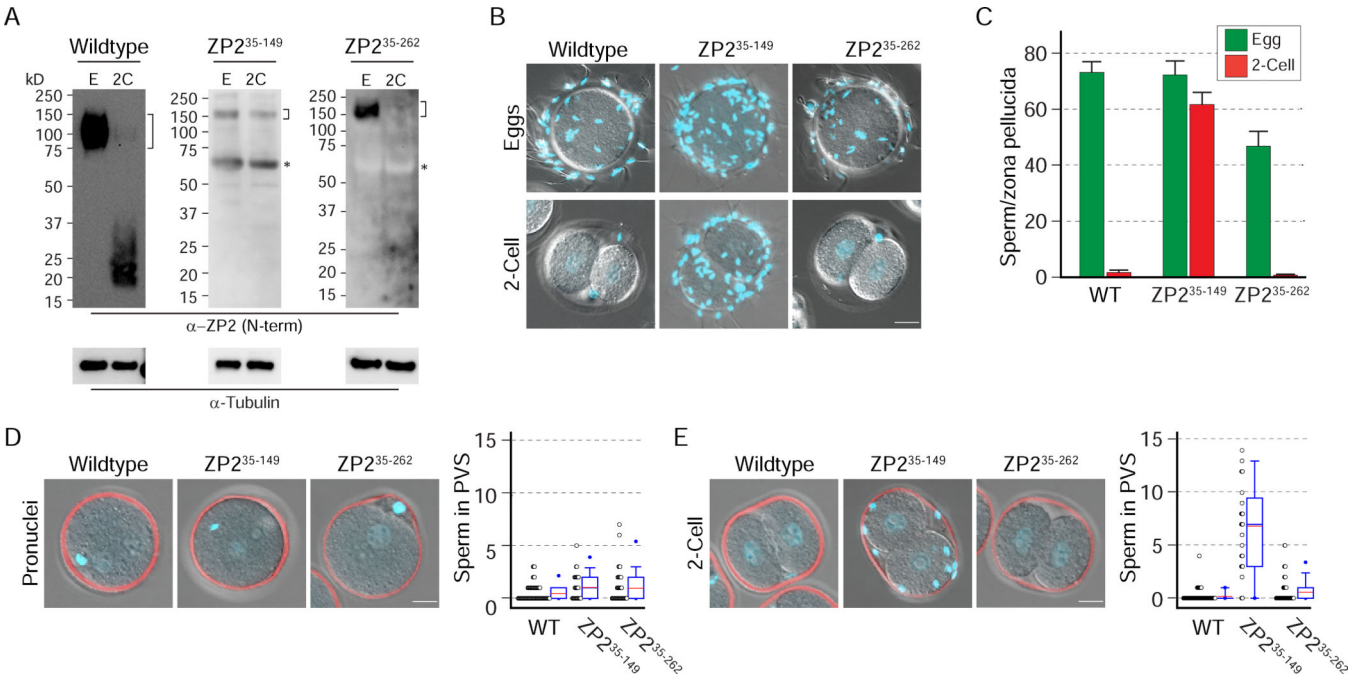

Figure 4. The penetration block dissipates and supernumerary sperm accumulate, if ZP2 is not cleaved

(A) Immunoblots of eggs (E) and two-cell embryos (2C) from wildtype and rescue mice augmented with hu*ZP4* to provide a more robust zona pellucida were probed with a monoclonal antibody to ZP2$^{N\text{-term}}$. The number/lane of eggs and embryos from wildtype (left), mo*Zp2*$^{35-149}$/hu*ZP4* (middle) and mo*Zp2*$^{35-262}$/hu*ZP4* (right) were 10, 100 and 200, respectively. Brackets, moZP2 or moZP2/huZP4 fusion protein. Asterisk, huZP4. Molecular mass, left. Anti-tubulin antibody staining (below) was used as a load control and to ensure protein integrity.

(B) Images of capacitated mouse sperm binding to the zona pellucida surrounding wildtype, mo*Zp2*$^{35-149}$/hu*ZP4* and mo*Zp2*$^{35-262}$/huZ*P4* rescue eggs (upper) and two-cell embryos (lower). Scale bar, 20 μm.

(C) Quantification from z-projections of sperm binding (mean ± s.e.m.) to eggs/embryos in (B). (D) Zona penetration after 6 hr incubation of mouse sperm with MII eggs from wildtype, mo*Zp2*$^{35-149}$/hu*ZP4* and mo*Zp2*$^{35-262}$/huZ*P4* rescue mice. For each genotype, images (left) and paired dot density and box plots (right) as described for Figure 3D. Scale bar, 20 μm.

(E) Same as (D), but with two-cell embryos. Scale bar, 20 μm.

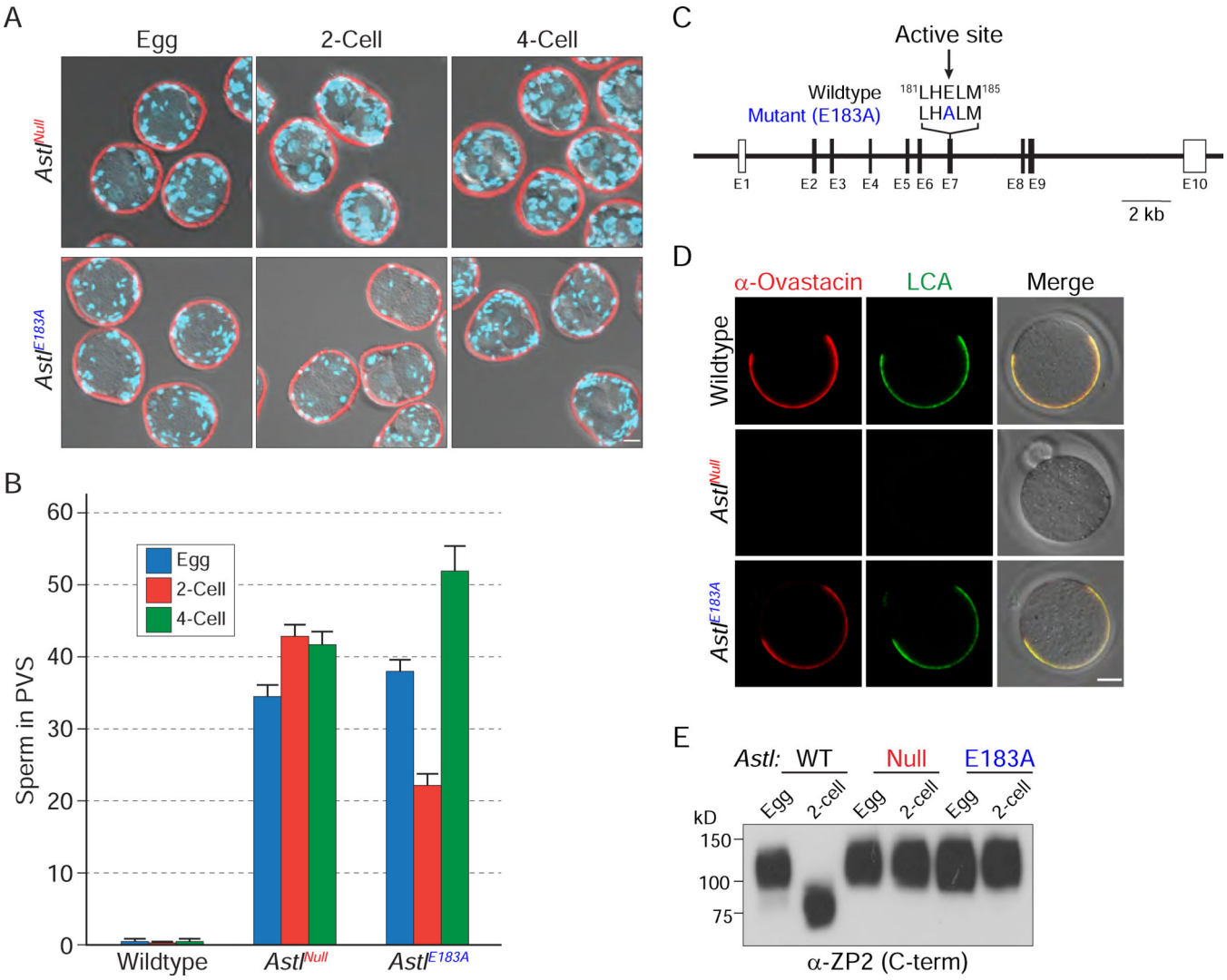

Figure 5. Ovastacin enzymatic activity is required for the transient block to zona penetration

(A) Unfertilized eggs, two- and four-cell embryos from *Astl*^{Null} and *Astl*^{E183A} rescue mice were incubated with capacitated sperm (5×10^5 ml^{-1}) for 6 hr. After washing with a wide-bore pipette to remove residual sperm on the zona surface, tissues were fixed, stained with WGA conjugated Alexa Flour 633 to visualize the zona pellucida, Hoechst 33342 to detect sperm nuclei and imaged by confocal microscopy. Scale bar, 20 μm.

(B) Quantification of the number of supernumerary sperm from (A) in the PVS of wildtype, *Astl*^{Null} and *Astl*^{E183A} rescue eggs, two- and four-cell embryos (mean ± s.e.m.). Wildtype data from Figure 3F.

(C) Exon map of *Astl*, a single-copy gene on mouse Chromosome 2 that encodes ovastacin, a zinc metallopeptidase. Arrow, CRISPR/Cas9 mediated mutation of the active site (E183A).

(D) Unfertilized eggs from wildtype, *Astl*^{Null} and *Astl*^{E183A} rescue mice were imaged by confocal microscopy after staining with rabbit anti-ovastacin antibody (left), LCA-FITC (a marker of cortical granules, middle) and merged with differential interference contrast (DIC) images (right). Scale bar, 20 μm.

(E) Immunoblot of lysates from eggs (10) and two-cell embryos (10) from wildtype, *Astl*^{Null} and *Astl*^{E183A} rescue mice probed with mAb specific for the C-terminal region of mouse ZP2 (m2c.2). Intact ZP2 is 120 kD and the cleaved C-terminal fragment of ZP2 is 90 kD. Molecular mass, left.

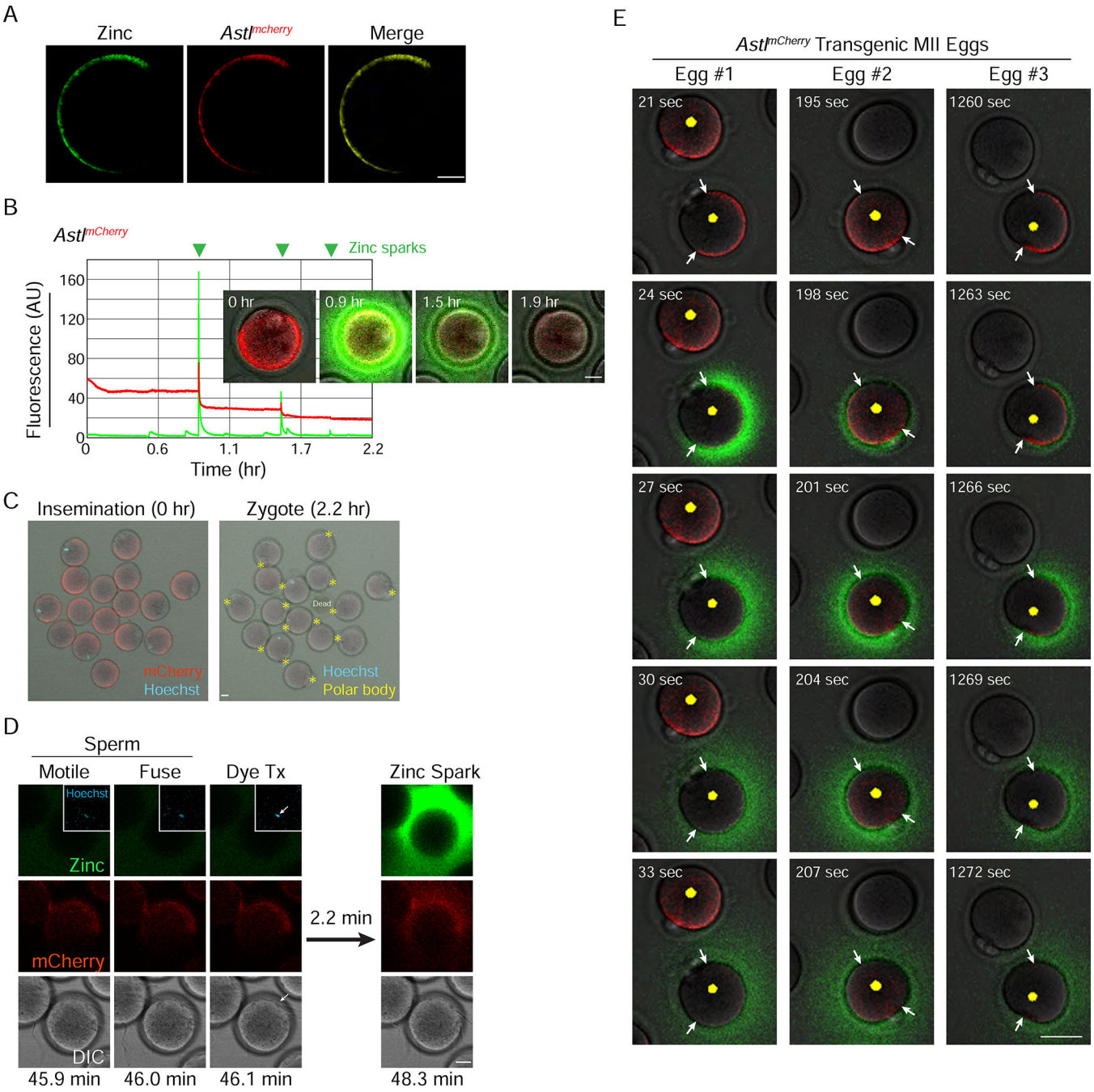

Figure 6. Release of zinc from MII eggs

(A) Confocal images of ovulated eggs from *Astl*^{mCherry} after staining with cell-permeable ZincBY-1. Single optical sections co-localized zinc (left) and ovastacin^{mCherry} (middle) in a merged image (right). Scale bar, 20 μm.

(B) Zinc sparks were observed in eggs from *Astl*^{mCherry} mice using FluoZin-3 tetrapotassium salt, a cell-impermeable zinc indicator, after induction of egg activation by $SrCl_2$. Images were obtained at the moment of a zinc spark or at the indicated time point.

Graph shows the relative signal intensities (AU) ovastacin^{mCherry} (red) and extracellular zinc (green) fluorescence. Inverted green triangles, zinc sparks. Scale bar, 20 μm.
(C) Zona-free, *Astl*^{mCherry} eggs were pre-loaded with Hoechst 33342, incubated with impermeant FluoZin-3 tetrapotassium salt and inseminated *in vitro* with capacitated epididymal sperm. Continuous confocal images were obtained for 2.2 hr at which time fertilized eggs were present as 1-cell zygotes with second polar body (asterisks, yellow). Scale bar, 20 μm.
(D) As in (C) with single egg resolution images for zinc (top), ovastacin^{mCherry} (middle) and DIC (bottom). Insets in top row, Hoechst 33342 to detect gamete fusion. Time points, bottom. Delay from gamete fusion (3rd column) to zinc spark (4th column), 2.2 min. Scale bar, 20 μm. (E) Time lapse recording (top to bottom in each columns) of zinc release from cortical granules after strontium-induced activation of MII eggs. Zinc sparks were detected by a cell-impermeable zinc indicator, FluoZin-3 tetrapotassium salt (green fluorescent) overlying cortical granules in *Astl*^{mCherry} (yellow dots) but not *Astl*^{Null} (unmarked) eggs. Arrows, borders of cortical granule free zone. Scale bar, 50 μm.

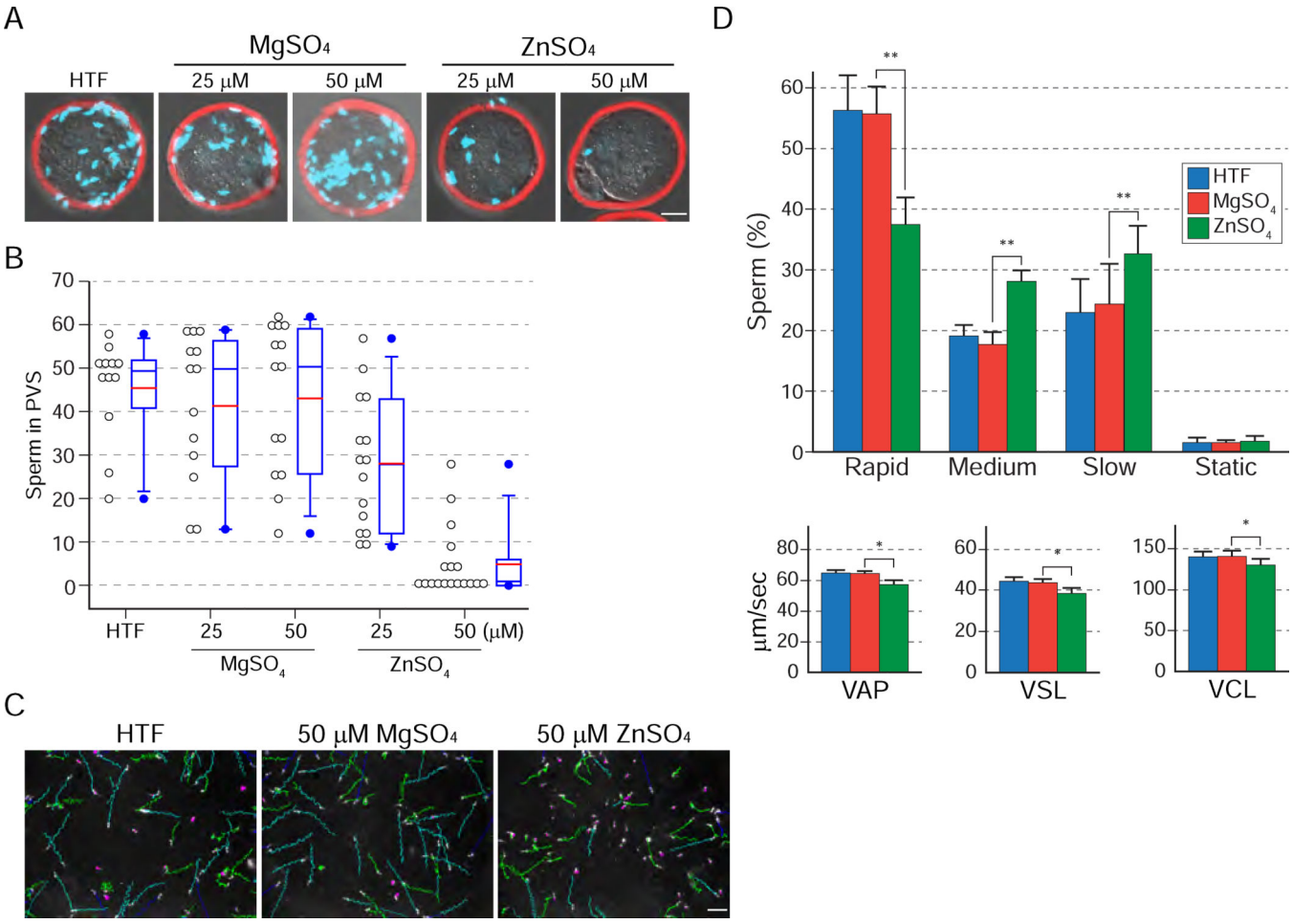

Figure 7. Effect of zinc on zona pellucida penetration and sperm motility

(A) Using *Astl*^{Null} eggs, *in vitro* fertilization was performed in HTF medium with 25 μM or 50 μM $ZnSO_4$ with capacitated sperm (5×10^5 ml^{-1}). The same concentrations of $MgSO_4$ were used as negative controls. After incubation (6 hr), eggs were fixed in paraformaldehyde, stained with Hoechst 33342 and WGA conjugated Alexa Fluor 633, and imaged. Scale bar, 20 μm. (B) Quantification of (A) from z-projections to determine the number of sperm in the PVS. For each concentration, paired dot density (left) and box (right) plots as described for Figure 3D. (C) Images of sperm tracks in HTF alone (left) or supplemented with 50 μM $MgSO_4$ (middle) or with 50 μM $ZnSO_4$ (right) analyzed with HTM-IVOS. Each colored sperm track showed rapid (light blue), medium (green), slow (pink) and static (red) movement. Dark blue tracks indicate sperm that move in and out of the focal plane. Scale bar, 100 μm.

(D) Capacitated sperm motility after incubation (2 hr) in HTF alone or supplemented with 50 μM $MgSO_4$ or $ZnSO_4$ grouped from (C) into rapid, medium, slow, and static sperm (upper). Distribution of sperm motility patterns from 4 independent experiments using three CASA parameters. VAP, Average Path Velocity; VSL, Straight Line Velocity; and VCL, Curvilinear Velocity. Mean ± s.e.m. The 2-tailed Student's t-test determined statistical differences, ** P <0.005, * P <0.05.

KEY RESOURCES TABLE

REAGENT or RESOURCE	SOURCE	IDENTIFIER
Antibodies		
Rat monoclonal anti-ZP1 (M1.4)	Jurrien Dean/ATCC	(Rankin et al., 1999)
Rat monoclonal anti-ZP2, N-terminus (IE-3)	Jurrien Dean/ATCC	(East and Dean, 1984)
Rat monoclonal anti-ZP2, C-terminus (m2c.2)	Jurrien Dean	(Rankin et al., 2003)
Rat monoclonal anti-ZP3 (IE-10)	Jurrien Dean/ATCC	(East et al., 1985)
Mouse monoclonal anti-human ZP4	Satish K. Gupta	(Bukovsky et al., 2008)
Rabbit polyclonal anti-ovastacin	Jurrien Dean	(Burkart et al., 2012)
Rabbit polyclonal anti-α-tubulin	MBL	Cat# PM054; RRID: AB_10598496
Goat anti-rat IgG (H+L) cross-absorbed secondary antibody conjugated Alexa Fluor 488	Thermo Fisher Scientific	Cat# A-11006; RRID:AB_2534074
Goat anti-mouse IgG (H+L) cross-absorbed secondary antibody conjugated Alexa Fluor 488	Thermo Fisher Scientific	Cat# A-11001; RRID:AB_2534069
Affipure F(ab')^2 fragment goat anti-rat IgG (H+L) conjugated horseradish peroxidase	Jackson ImmunoResearch Labs	Cat# 112–036-062; RRID:AB_2338142
Affipure F(ab')^2 fragment goat anti-rabbit IgG (H+L) conjugated horseradish peroxidase	Jackson ImmunoResearch Labs	Cat# 111–036-045; RRID:AB_2337943
Bacterial and Virus Strains		
BAC DNA (RP23–6513)	Thermo Fisher Scientific	Clone#: RP23–6513
BAC DNA (RP11–484B19)	CHORI	Clone#: RP11–484B19
SW102	Donald L. Court	(Warming et al. 2005)
Chemicals, Peptides, and Recombinant Proteins		
PNGase F	New England BioLabs	Cat# P0704S
FluoZin-3, tetrapotassium salt (impermeant)	Thermo Fisher Scientific	Cat# F24194
FluoZin-3, AM (permeant)	Thermo Fisher Scientific	Cat# F24195
ZincBY-1 (permeant)	Imaging Probe Development Core, NHLBI	(Que et al., 2014)
Wheat germ agglutinin (WGA) conjugated Alexa Fluor 633	Thermo Fisher Scientific	Cat# W21404
Lectin from lens culinaris conjugated FITC	Sigma Aldrich	Cat# L9262
Strontium chloride	Sigma Aldrich	Cat# 439665
Magnesium sulfate heptahydrate	Sigma Aldrich	Cat# 230391
Zinc sulfate heptahydrate	Sigma Aldrich	Cat# Z0251
HTF medium	Zenith Biotech	Cat# ZHTF-100
M2 medium	Zenith Biotech	Cat# ZFM2–100
KSOM medium	Zenith Biotech	Cat# ZEKS-050
Bovine serum albumin	Equitech-Bio, Inc.	Cat# BAC62
Critical Commercial Assays		
PrimeScript RT reagent kit	Takara Bio USA	Cat# RR037A
AmpliScribe T7-flash transcription kit	Lucigen	Cat# ASF3257
mMESSAGE mMACHINE T7 ULTRA transcription kit	Thermo Fisher Scientific	Cat# AM1345

REAGENT or RESOURCE	SOURCE	IDENTIFIER
MEGAclear transcription clean-up kit	Thermo Fisher Scientific	Cat# AM1908
Experimental Models: Organisms/Strains		
Mouse: *Zp2*^{Null}	Jurrien Dean/MMRRC	(Rankin et al., 2001)
Mouse: *Astl*^{Null}	Jurrien Dean/MMRRC	(Burkart et al., 2012)
Mouse: Tg (*Zp2*^{Mut})	Jurrien Dean/MMRRC	(Gahlay et al., 2010)
Mouse: Tg (*Astl-mCherry*)	Jurrien Dean/MMRRC	(Xiong et al., 2017)
Mouse: Tg (hu*ZP4*)	Jurrien Dean/MMRRC	(Yauger et al., 2011)
Mouse: Tg (mo*Zp2*$^{35-149}$/hu*ZP4*)	This paper	N/A
Mouse: Tg (mo*Zp2*$^{35-262}$/hu*ZP4*)	This paper	N/A
Mouse: Tg (mo*Zp2*$^{35-149(N83Q)}$/hu*ZP4*)	This paper	N/A
Mouse: Tg (*Zp2*^{N83Q})	This paper	N/A
Mouse: *Astl*^{E183A}	This paper	N/A
Oligonucleotides		
Primers to produce and evaluate transgenes, see Table S2	This paper	N/A
Primers to produce sgRNA expression plasmid and single strand DNA for *Astl*^{E183A} mouse line, see Table S3	This paper	N/A
Primers for genotyping, see Table S4	This paper	N/A
Primers for RT-PCR, see Table S5	This paper	N/A
Recombinant DNA		
MLM3613 for Cas9 mRNA synthesis	(Hwang et al., 2013)	Addgene #42251
pUC57-sgRNA expression vector for sgRNA synthesis	(Shen et al., 2014)	Addgene #51132
Pl253 plasmid	Donald L. Court	(Liu et al., 2003)